AIP | The Journal of Chemical Physics

Band structure, crystal conformation, and hydrogen bond potentials for solid HF

Alex Zunger

Citation: The Journal of Chemical Physics **63**, 1713 (1975); doi: 10.1063/1.431568
View online: http://dx.doi.org/10.1063/1.431568
View Table of Contents: http://scitation.aip.org/content/aip/journal/jcp/63/5?ver=pdfcov
Published by the AIP Publishing

Band structure, crystal conformation, and hydrogen bond potentials for solid HF

Alex Zunger

Department of Theoretical Physics, Soreq Nuclear Research Centre, Yavne, Israel
Department of Chemistry, Tel Aviv University, Tel Aviv, Israel

(Received 27 August 1974)

The electronic structure of hydrogen fluoride chains is calculated using the small-periodic-cluster approach by representing some high-symmetry points in the Brillouin zone of the infinite solid by the one-electron energies of a finite periodic structure. The LCAO representation is used for the crystal orbitals, and a self-consistent calculation is performed. Problems regarding the convergence of the band structure as a function of the number of K-grid points used to construct the Hartree–Fock elements, the number of interacting neighbors, and the approach to self-consistency in the iteration cycle are examined. Band energies, ionization potential, cohesive energy, charge, and electrostatic potential distribution are computed. The adequacy of other methods currently used to investigate electronic and structural problems in hydrogen-bonded solids is discussed in view of the results obtained. The crystal structure is optimized, and the stability of the crystal against unit cell deformations and atom displacements is examined. Potentials for either collective or single proton movements are computed and discussed in view of the experimental vibrational force constants.

I. INTRODUCTION

The electronic and structural properties of hydrogen bonds in solids are usually treated by one of the following approaches:

(a) The perfect lattice is treated by a tight binding model, considering the crystalline potential as a superposition of unperturbed isolated molecule electrostatic potentials.[1,2]

(b) The elementary A–H. . . B hydrogen bond moiety in the solid is considered by calculating various properties of isolated dimers. This has been treated by either electrostatic models of point-charge interaction[3–5] and charge-distribution interactions,[6,7] or by quantum-mechanical models based on valence-bond representations,[8,9] charge-transfer theories[10,11] or self-consistent molecular-orbital (SCF–MO)[12–15] techniques.

(c) To account for charge-redistribution effects experienced by molecules in hydrogen-bonded solids and to obtain a quasibandlike picture of the one-electron energy levels, truncated-crystal approaches have been used. In these representations, highly-truncated clusters (trimers, pentamers, and hexamers) are considered by various linear combinations of atomic orbitals (LCAO) techniques,[16–18] and the convergence behavior of the electronic properties is examined as a function of the cluster size.

(d) Conformational and lattice-dynamical aspects of hydrogen-bonded solids have been treated via semiempirical atom–atom or bond–bond pair potentials[19–24] using extensive parametrization to obtain the experimental bond lengths, cohesive energy, and, in some cases, vibrational frequencies.

The non-self-consistent tight-binding approach (a) has the advantage of describing the true extended periodic character of the charge distribution and the electronic states of the crystal; however, it neglects both the polarization effects experienced by each molecule in its hydrogen-bonded crystalline environment and the charge redistribution in the solid relative to the isolated molecule. Investigation of the polarization energies of pairs of molecules forming moderate to strong hydrogen bonds in solids indicates that these corrections may be of the same order of magnitude as the total H-bond energy.[25] SCF–MO calculations of various polymers of hydrogen-bonded molecules, on the other hand, have demonstrated that the molecular charge distribution might be changed by as much as 30%–50% relative to the isolated molecular values,[17,18,26,27] these charge-redistribution effects having a predominant influence on the electronic properties of the hydrogen-bonded system. Also, the tight-binding model, relying heavily on the translational symmetry of the lattice, is inadequate for treating the stability of a given solid structure against displacements of atoms from their ideal lattice sites and for obtaining potentials for proton motion.

In approach (b), a relatively small number of atoms is treated via *ab initio* methods to give accurate results regarding charge distributions, conformations, hydrogen-bond potentials, and interaction energies. However, the relevance of this approach is limited mainly to isolated dimers in the gas phase, while molecular pairs both in solids and in biological macromolecules are usually strongly coupled to their environment. The treatment of the fully coupled solid systems by *ab initio* methods is presently difficult to implement in practice owing to computation-effort considerations.

The truncated-crystal approach (c) presents a systematic method of accounting for the deficiencies in the isolated-dimer picture but sacrifices the accuracy of the one-electron methods employed, to some extent, by applying semiempirical rather than *ab initio* LCAO techniques. Truncated-crystal methods were shown to be successful when applied to predominantly covalent bonded structures, like diamond,[28,29] graphite,[30] and boron nitride,[30] where the perturbations exerted by the cluster surfaces do not propagate too deeply into the bulk. Similar calculations on hydrogen-bonded solids,[17,18] on the other hand, reveal substantial charge inhomogenities inside the cluster due to the large electron delocalization and charge-redistribution effects, characterizing the hydrogen-bonded systems. Owing to these strong perturbations, lattice periodicity could not be simulated, and the atomic charges and electronic eigenvalues obtained were not correlated with corresponding properties in a regular periodic structure.

The phenomenological atom–atom potential approach (d) has the advantage of representing structural properties and potentials for proton movements in infinite-periodic structures, thereby correlating various hydrogen-bond properties of many solids. Its applicability is, however, limited by the availability of sufficient experimental data to determine the values of the adjustable parameters, and thus only the most common O–H· · ·O and N–H· · ·O=C bonds were considered. Owing to the absence of sufficient experimental data to parametrize the intramolecular force field, the phenomenological atom–atom methods that were directly applied to hydrogen-bonded solids[21–24] considered the hydrogen-bond formation as a purely intermolecular process, with the molecules in the solid held rigidly, usually in their gas-phase conformation. This approximation seems questionable in view of the significant intramolecular rearrangements that have been shown to occur upon hydrogen-bond formation in solids as determined in neutron-diffraction studies, nuclear magnetic resonance (NMR), and in vibrational analysis.[31–33] Since, in this model, the elementary pair interaction is assumed to depend only on the atomic positions, keeping the potential parameters fixed for all distances, many-body effects are neglected. On the other hand, quantum-mechanical treatments,[34] allowing for different polarizations of the protons at different positions, indicate a rather pronounced collective effect of all protons on the potential between a given atom pair.

Recently, we proposed a method for self-consistently treating the electronic structure of both perfect periodic solids[35] and point defect problems.[36] The method is based on the representation of some high-symmetry points in the Brillouin zone (BZ) of the solid by the one-electron spectrum of small periodic clusters of atoms, using LCAO representation. Edge effects are completely suppressed by employing periodic boundary conditions, and a self-consistent procedure is used to modify the isolated molecule potential in the crystalline environment. The cluster wavefunctions are not explicitly constrained to be periodic, but rather, their transformation properties are determined by the arrangement of the cluster atoms, permitting both a periodic solution (when the atoms are periodically arranged) and a defect-superlattice solution (when a defect is placed at the center of a large Born Von Karman cell).

In this paper and in Ref. 37, the method is applied to hydrogen bonds in solids. We treat the band structure, hydrogen-bond potentials, and ionic-defect structures in solid HF. Approaches (a)–(d) are discussed with reference to this method.

II. METHOD OF CALCULATION

A. Small periodic cluster (SPC) approach

The method will first be illustrated on a one-dimensional crystal. Extensions to more than one dimension are straightforward[35,36] and will be mentioned later.

Consider a one-dimensional chain of arbitrary conformation (linear, zigzag, etc.) made up of atoms of either identical or different chemical species (molecular chain) with atomic orbitals $\chi_\mu(\mathbf{r}-\mathbf{R}_n)$ centered on each site n, where $\mu = 1 \ldots \sigma$ denotes the atomic basis function ($1s$, $2s$, $2p_x$, $2p_y$, $2p_z$). The interaction radius (maximum separation between two atoms for which the interaction potential is still considered nonzero) is denoted by R_c. The lattice is divided into Born Von Karman (BVK) cells (Fig. 1), each containing either an even ($2N$) or odd ($2N+1$) number of atoms. In the LCAO representation, the electronic wavefunction of one such cell is given (e.g., for an odd number of atoms) by

$$\psi_j = \sum_{\mu=1}^{\sigma} \sum_{n=1}^{2N+1} C_{\mu n j}\, \chi_\mu(\mathbf{r}-\mathbf{R}_n), \quad j = 1 \ldots \sigma(2N+1), \tag{1}$$

where $C_{\mu n j}$ are the LCAO expansion coefficients. We wish to find the eigenvector coefficients $\{C_{\mu n j}\}$ and the energy eigenvalues E_j for the electronic secular equations describing this cell, in the field of all other similar BVK cells in the crystal with no edge effects, i.e., an array in which any atomic species on a given sublattice experiences a field identical with that of all other atoms on equivalent sites. This may be accomplished by extending the BVK cell by atoms labelled $1 \cdots N$ on one side, and atoms $(N+2) \cdots (2N+1)$ on the other side (Fig. 1) and considering the electronic eigenvalue problems of the central BVK cell, where the interaction between any given pair of atoms, either intracell or intercell, is taken to be that of the pair joined by the shortest path, subjected to the condition that $R_c \leq |R_n - R_m|$, where $(n-m) = N+1$. For a one-dimensional lattice of $2N+1$ atoms, interactions up to N neighbors can thus be considered.

The variational equations for the $(2N+1)$-atom cluster are given by

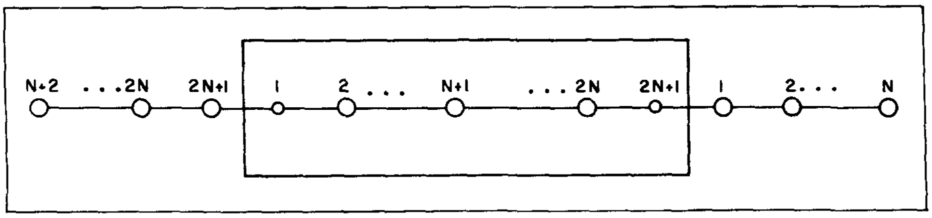

FIG. 1. Central unit cell (rectangular frame) and the atoms outside it used to obtain periodic connections.

$$\sum_{\mu=1}^{\sigma}\sum_{n=1}^{2N+1}\left[F_{\mu n,\lambda m}-S_{\mu n,\lambda m}E_j\right]C_{\mu nj}=0,$$

$$j=1\ldots\sigma(2N+1), \qquad (2)$$

and the matrix elements expressed in the atomic basis set, are

$$F_{\mu n,\lambda m}=\langle\chi_\mu(\mathbf{r}-\mathbf{R}_n)|\hat{F}|\chi_\lambda(\mathbf{r}-\mathbf{R}_m)\rangle, \qquad (3a)$$

$$S_{\mu n,\lambda m}=\langle\chi_\mu(\mathbf{r}-\mathbf{R}_n)|\chi_\lambda(\mathbf{r}-\mathbf{R}_m)\rangle \qquad (3b)$$

for $|R_n-R_m|\leq R_c$, and $F_{\mu n,\lambda m}=S_{\mu n,\lambda m}=0$ for $|R_n-R_m|>R_c$, where $\hat{F}$ is the one-electron Hartree–Fock operator.

Since the matrix elements $F_{\mu n,\lambda m}$ and $S_{\mu n,\lambda m}$ are determined, for a given basis set, by the positions and mutual orientation of the atoms in the cluster (the cluster's symmetry group), the geometrical periodicity that we have imposed on the interactions could be conveniently constructed by defining an interatom distance matrix $D^{(\eta)}$ and three interatom direction-cosine matrices with respect to arbitrary x, y, and z directions: $E_{(x)}^{(\eta)}$, $E_{(y)}^{(\eta)}$, and $E_{(z)}^{(\eta)}$. η denotes the maximal interaction order $R_c/|\mathbf{b}|$, where $\mathbf{b}$ is a primitive unit cell vector. $D^{(\eta)}$ is expressed in terms of the unit cell parameters, while $E_{(x)}^{(\eta)}$, $E_{(y)}^{(\eta)}$, and $E_{(z)}^{(\eta)}$ are expressed in terms of the molecular orientations in the unit cell. These four matrices define the interaction geometry of a pseudomolecule consisting of $2N+1$ (or $2N$) atoms. They are built to be periodic and with the symmetry properties of the investigated solid structure formed by translating the central BVK cell. For example, a seven-atom one-dimensional linear chain with a nearest neighbor distance $|\mathbf{b}|$ that is directed along the x direction has the interaction-geometry matrices (for three-orders of interaction)

$$D^{(3)}=|\mathbf{b}|\cdot\begin{vmatrix}0&1&2&3&3&2&1\\1&0&1&2&3&3&2\\2&1&0&1&2&3&3\\3&2&1&0&1&2&3\\3&3&2&1&0&1&2\\2&3&3&2&1&0&1\\1&2&3&3&2&1&0\end{vmatrix}\qquad E_{(x)}^{(3)}=\begin{vmatrix}0&&&&&&\\&0&&&\mathbf{1}&&\\&&0&&&&\\&&&0&&&\\&&&&0&&\\&-\mathbf{1}&&&&0&\\&&&&&&0\end{vmatrix} \qquad (4)$$

while $E_{(y)}^{(3)}$ and $E_{(z)}^{(3)}$ are identically zero. The elements in the upper right and lower left corners of $D^{(3)}$ denote the distances between atoms in the central BVK cell and those outside it which are used to establish the required periodicity, while the other elements denote the simple intracell distances. The elements of the Hartree–Fock energy and overlap matrices are constructed from the corresponding elements of these interaction-geometry matrices using a given basis set.

Several possible more general applications of the model are

(1) For general nonlinear structures, the $E^{(\eta)}$ matrices are expressed in terms of the angles defining the molecular orientation with respect to arbitrary x, y, and z directions (such as the chain angles, etc). These matrices are then built according to the given unit-cell symmetry group.

(2) For a unit cell with more than one atomic species, the $F_{\mu n,\lambda m}$ elements in Eq. (3) are expressed by the proper atomic orbitals belonging to the different atoms, and with the same interaction geometry matrices $D^{(\eta)}$ and $E^{(\eta)}$.

(3) The same method can also be used for two and three dimensional structures, now extending the central BVK cell in the x as well as in the y and z directions, in order to obtain periodicity in two or three dimensions, respectively.[35] The same restrictions on the number of atoms placed outside the cell and the maximum interaction range for a given size of the central BVK cell are used.

(4) The eigenvalue problem for a defect structure is similarly constructed.[36] A model for a substitutional impurity involves the change of the central $(N+1)$ row and the $(N+1)$ column in the **F** and **S** matrices, replacing them by the matrix elements describing the interaction of the impurity atom with the rest of the $2N$ atoms. The eigenvalue problem thus generated corresponds to a superlattice of impurities, where the separation between nearest impurity sites is larger than R_c and thus no direct impurity–impurity interaction is present. The superlattice picture should not place a severe restriction in comparing the results with experimental data for a low concentration of defects, since in most cases the isolated impurity limit could be approached to a good approximation by increasing the BVK cell size, thereby increasing the impurity–impurity distance.

(5) Since the number of the variational equations (2) was not reduced by imposing translational symmetry requirements (Bloch conditions) on the wavefunction in Eq. (1), it is possible to treat large deviations from translational symmetry (also in the dilute superlattice representation) by this method. Hence, the problems of relaxation of atomic positions (around a substitutional defect site or in the perfect lattice where stability of a given structure is examined against atom displacement) are treated within the model by changing one row and one column in the $D^{(\eta)}$ and $E^{(\eta)}$ matrices and generating the corresponding new **F** and **S** matrices which now reflect a local change in geometry.

The difference between the defect and local relaxation problems on one hand and the perfect lattice problem on the other lies in the fact that in the latter case the eigenvalues $E_j = E_{\gamma,p} (\gamma = 1, .., \sigma h;\ p = 0 \cdots 2N/h)$ can be classified according to the wave vector $\mathbf{K}_p$ in the BZ generated from the primitive unit cell of the solid investigated. This can be done by recognizing that for a perfect periodic arrangement of the atoms,

$$E_{\gamma,p} = E_\gamma(\mathbf{K}_p), \quad \text{where } p = 0, 1 \ldots, (2N/h),$$
$$C_{\mu n j} \equiv C_{\mu n,\gamma p} = C_{\mu\gamma}(\mathbf{K}_p) e^{i\mathbf{K}_p \cdot \mathbf{R}_n}, \tag{5}$$
$$\mathbf{K}_p = \frac{2\pi}{(2N+1)\mathbf{b}} \cdot p.$$

Therefore, in the solution of Eqs. (1)–(3) for a perfect lattice, one obtains a finite subset of the full eigenvalue spectrum of the infinite solid under investigation. The size of this subset is determined only by the number of primitive unit cells inside the central BVK cell $(2N+1)/h$, where h denotes the number of molecules in a primitive unit cell. The eigenvalues obtained correspond to wave vectors $\mathbf{K}_p$ that are evenly spread in the BZ [Eq. (5)].

Owing to the periodicity of the structure, surface effects and charge inhomogeneity, which characterize truncated-crystal models,[17a,18] are completely eliminated. The fact that the band structure $E_\gamma(\mathbf{K}_p)$ is evaluated only at a discrete set of $(2N+1)/h$ points in the BZ is an inherent limitation of the model, and thus density of state functions could be considered only in the form of a histogram. However, for a managable cluster size ($2N \sim 20$–40 atoms), most of the high-symmetry points in the BZ that are relevant in discussing optical properties of the solid could easily be obtained.

The matrix elements of the Hartree-Fock operator are given by

$$F_{\mu n,\lambda m} = H_{\mu n,\lambda m} + \sum_{\mu' s \lambda' t} P_{\mu' s \lambda' t} \times [(\mu n \lambda m \mid \mu' s \lambda' t) - \tfrac{1}{2}(\mu n \lambda' t \mid \lambda m \mu' s)], \tag{6}$$

where the core part is given by

$$H_{\mu n,\lambda m} = \langle \chi_\mu(\mathbf{r}_1 - \mathbf{R}_n) \mid -\tfrac{1}{2}\nabla^2 - \sum_s \sum_A \frac{Z_A}{\mathbf{r}_{1A} - \mathbf{R}_A^s} \mid \chi_\lambda(\mathbf{r}_1 - \mathbf{R}_m)\rangle, \tag{7}$$

and the two-electron matrix elements are

$$(\mu n \lambda m \mid \mu' s \lambda' t) = \langle \chi_\mu(\mathbf{r}_1 - \mathbf{R}_n)\chi_\lambda(\mathbf{r}_1 - \mathbf{R}_m) \mid \frac{1}{r_{12}} \mid \chi_{\mu'}(\mathbf{r}_2 - \mathbf{R}_s)\chi_{\lambda'}(\mathbf{r}_2 - \mathbf{R}_t)\rangle. \tag{8}$$

The subscript on the electronic coordinate $\mathbf{r}_i$ numbers the electron and Z_A is the nuclear charge of atom A. The elements $P_{\mu' s,\lambda' t}$ of the charge-density matrix are given by the eigenvector expansion coefficients $C_{\mu' s j} \equiv C_{\mu' s \gamma p}$ in one of the following two forms:

$$P_{\mu' s \lambda' t} = 2 \sum_{p=0}^{2N/h} \sum_{\gamma=1}^{\sigma_{\mathrm{occ}}} C^*_{\mu' s \gamma p} C_{\lambda' t \gamma p} \tag{9}$$

or, in the $\mathbf{K}$ representation for a perfect periodic structure,

$$P_{\mu' s \lambda' t} = 2 \int_{\mathbf{K}_p} \sum_{\gamma=1}^{\sigma_{\mathrm{occ}}} C^*_{\mu' \gamma s}(\mathbf{K}_p) C_{\lambda' \gamma t}(\mathbf{K}_p) \exp[i\mathbf{K}_p \cdot (\mathbf{R}_s - \mathbf{R}_t)] d\mathbf{K}_p, \tag{10}$$

where σ_{occ} denotes the number of occupied bands in the ground state. It is obvious that the $F_{\mu n,\lambda m}$ matrix elements depend not only on the pair $\mu n, \lambda m$ but also on all occupied bands extending over all the atoms [Eqs. (6) and (9)] or alternatively on all occupied bands at all the $\mathbf{K}_p$ values spanning the BZ [Eqs. (6) and (10)]. This makes the problem a self-consistent one and necessitates the recompilation of the crystal potential matrix elements $F_{\mu n,\lambda m}$ on the basis of the calculated band structure [Eq. (9) or (10)] at each iteration. One therefore guesses the elements of the charge-density matrix (for predominantly covalent structures, the neutral free-atom charge distribution is used, while for ionic and metallic solids the free-ionic charge distribution is used), computes the Hartree–Fock matrix elements [Eq. (6)] by evaluating the two-electron integrals [Eq. (8)] and the core Hamiltonian elements [Eq. (7)], calculates the overlap matrix elements [Eq. (3b)], and solves Eq. (2) for the expansion coefficients. The charge-density matrix is then recalculated for σ_{occ} occupied bands (in metals, this necessitates the calculation of the Fermi energy for each iteration to determine the occupied levels), and this is used to construct a refined F matrix. The process is terminated either when the difference in the charge-density matrix in two successive iterations is within a certain tolerance level or when the eigenvalue spectrum reaches convergence within a prescribed limit. During iteration, only the $\mathbf{P}$ matrix is varied by successive diagonalization of Eq. (2), while other quantities [Eq. (7), Eq. (8), and Eq. (3b)] are stored. The energy spectrum of the system is specified by $E_\gamma(\mathbf{K}_p)$ for each band γ in a perfect periodic structure or by $E_{\gamma,p}$ for any arbitrary defect structure.

The total electronic energy is given by

$$E_{\mathrm{elec}} = \frac{1}{2} \sum_{\mu n \lambda 0} P_{\mu n \lambda 0} [H_{\mu n \lambda 0} + F_{\mu n \lambda 0}] \tag{11a}$$

and the nuclear energy by

$$E_{\mathrm{nuc}} = \sum_{A<B} \frac{Z_A Z_B}{R_{AB}}. \tag{11b}$$

The total energy is obtained by adding the nuclear–nuclear interactions to the total electronic energy. Stabilization energies are calculated as the difference between total energy per atom (or molecule) and the energy of an isolated atom (or molecule). The crystal equilibrium conformation is obtained by minimizing the total energy with respect to both the unit cell parameters and the atomic positions inside the unit cell. Force constants are obtained by performing appropriate numerical derivatives of the total energy, in the vicinity of the equilibrium conformation, with respect to dynamical displacement coordinates in the crystal.

The charge-density matrix obtained in the last iteration is subjected to an electron population analysis[38] to obtain net and orbital atomic charges. Exchange terms appearing in Eq. (6) are directly evaluated as in molecular calculations without using statistical local $X\alpha$ exchange.[39] Self-consistent charge redistribution is allowed for the intermolecular and intramolecular regions, while in both the molecular tight binding scheme recently suggested[1] and in the self-consistent augmented-plane-wave (APW) method,[40] only the intramolecular and atomic sphere regions, respectively, are self-consistently treated. Spherical averaging of the potential within each molecule[1] is unnecessary in the SPC method, and the directionality of the chemical bonds in the molecular crystal is automatically preserved.

The convergence problems that have to be studied in this scheme are

(a) Number of grid points in **K** space used to reevaluate the charge density matrix [Eq. (9)] in a given iteration;

(b) Number of neighbors included in the evaluation of the $F_{\mu n,\lambda m}$ and $S_{\mu n,\lambda m}$ elements [the value of R_c in Eq. (3)];

(c) Number of self-consistency iterations used to converge either the density matrix or the band structure. Owing to computational difficulties with larger basis sets, the convergence of the sum in Eq. (1) as a function of the number of basis orbitals used will not be examined, and a valence basis set will be used throughout.

It should be mentioned that the two convergence problems (a) and (b) could be reduced to one in this scheme by taking the largest interaction radius R_c permitted for a given size of the central BVK cell. In this way, the number of interactions and the number of **K** values used are determined uniquely by the cluster size.

Other self-consistent schemes for energy-band calculations employing a reciprocal-space rather than a direct real-space representation have been attempted in recent years, within the APW approach,[40] the orthogonalized-plane-wave (OPW) approach,[41] and the tight-binding approach.[39] However, none of these methods have previously been applied to both perfect lattices and defect problems, these being treated at different levels of approximations. Point defect properties have been treated either with various perturbative schemes based on the zero order lattice periodic states[42] or by the local orbitals surrounding the defect site, neglecting the rest of the lattice.[43] The first approach, being perturbative, fails to treat lattice relaxations around the defect site that introduce marked changes in the electronic structure. Only limited information regarding the charge distribution around the defect site has been obtained by this method. The second approach, considering only the local environment of the defect, does not account for the coupling of the defect with the bulk crystal through delocalization effects and fails to relate the defect levels with the edges of the crystal bands. Effective-mass approximations, on the other hand, are usually not suitable for deep defect levels with large interaction radii, encountered in many insulator and semiconductor defect studies.

B. Choice of the LCAO approximation

Since there are indications that the properties of the hydrogen bond in solid HF are determined not only by short range but also by considerably long range forces,[34] even a one-dimensional model for the solid would involve solutions of eigenvalue problems for clusters of 20–40 atoms in the SPC approach. Such calculations are presently difficult to implement at the *ab initio* level, even with minimal basis sets, and one is forced to consider some form of approximate LCAO schemes for evaluating the various terms in Eq. (6).

Extended Hückel calculations have been carried out on some hydrogen-bonded systems.[44] Since considerable charge transfer is involved in HF aggregates,[17,18] such a non-self-consistent LCAO scheme could not be used.[45] The CNDO/INDO methods[46] using a valence basis set of Slater orbitals (1*s* for hydrogen and 2*s* and 2*p* for fluorine) have been shown to reasonably reproduce *ab initio* calculated and experimentally measured properties of both the isolated HF molecule and linear dimers of HF. The results of such calculations are summarized in Tables I and II, respectively.

It is evident that charge distribution and one-electron energy levels of the monomer are favorably described by the INDO method, while the dimer interaction energy seems to be overestimated. Intermolecular orbital overlap and configuration interaction, which are neglected in this scheme, are probably responsible for this shortcoming.[30b] The over-all agreement between INDO

TABLE I. Calculated and experimental properties of the HF molecule. E_0 denote the ground state Hartree–Fock total energy.

Property	INDO	Exptl	Minimal basis set	Extended basis set
Fluorine net charge (e)[a]	−0.268	⋯	−0.225[b]	−0.230[c]
Dipole moment (D), (H^+F^-)	1.99	1.82[d]	1.39[b] 0.878[e] 1.44[e′]	1.827[c] 2.382[f] 1.934[g]
Quadrupole moment (esu × 10^{-26})	1.56[h]	2.6[i]	3.05[j] 2.46[j′]	2.33[g]
Bond length (Å)	1.006	0.917[k]	0.9384[b]	0.916[f] 0.917[g]
Dissociation energy (eV)	6.30	6.12[l]	1.21[e] 2.56[e′]	4.44[g] 4.114[c]
E_{π} (eV)	19.96	19.05[m]	12.64[e] 12.75[e′]	17.70[g]
$E_{3\sigma}$ (eV)	21.70		15.39[e] 16.47[e′]	20.91[g]
$E_{2\sigma}$ (eV)	44.16		40.17[e] 40.51[e′]	43.57[g]
Force constant (dyn/cm × 10^{+5})	10.50	9.6[n]	⋯	13.18[c]

[a] Mulliken's definition.
[b] Reference 16, $E_0 = -99.270225$ a.u.
[c] Reference 47, $E_0 = -100.057127$ a.u.
[d] Reference 48.
[e] Reference 49, Slater orbitals, $E_0 = -99.47854$ a.u.; [e′] Ref. 49, best limited set, $E_0 = -99.53614$ a.u.
[f] Reference 17b, $E_0 = -100.01346$.
[g] Reference 50, $E_0 = -100.0705$ a.u.
[h] Reference 51.
[i] Reference 52.
[j] Reference 53, computed with wavefunctions (e); [j′] Ref. 53, computed with wavefunctions (e′).
[k] Reference 54.
[l] Reference 55.
[m] Reference 56.
[n] Reference 57.

TABLE II. Calculated values for the most stable HF dimer compared with experimental data. E_0 denotes the ground state Hartree–Fock monomer total energy. θ denotes the intermolecular angle and ΔE the stabilization energy.

Method	R_{HF} (Å)	R_{FF} (Å)	θ (deg)	ΔE(kcal/mole)
INDO	1.00	2.45	40.5	9.1
Minimal set[a]	0.9384[b]	2.55	69	5.20
Extended set[c]	0.946[b]	2.87	40	4.7
Extended set[d]	0.916[b]	2.78	20	6.48
Extended set[e]	0.917[b]	2.85	40	4.5
Experimental		2.79 ± 0.05[f]	20 ± 5[g] (60–70)[f]	6.0 ± 1.5[g]

[a] Reference 16, $E_0 = -99.270225$ a.u.

[b] R_{HF} distance not optimized for the dimer.

[c] Reference 17b, atomic basis set $E_0 = -99.99578$ a.u. with scaled hydrogens.

[d] Reference 17b, split-out atomic basis $E_0 = -100.01346$ a.u.

[e] Reference 58, $E_0 = -100.05638$ a.u.

[f] Reference 59.

[g] Reference 60.

and *ab initio* results is reasonable, and it is felt that the former method is presently an agreeable compromise between accuracy and computation-time costs involved in extensive band structure and structure-optimization calculations in solids. Hence, the method will be used with the SPC model throughout this paper.

III. BAND STRUCTURE AND CONVERGENCE EFFECTS

A. Band structure

Hydrogen fluoride crystallizes at − 83.4 °C in long zigzag chains. X-ray single crystal diffraction studies[61] could not distinguish between the space group D_{2h}^{17} with two molecules per unit cell, in which the sense of the chains is randomly distributed relative to the crystal y axis, and the ordered structure D_{2h}^{16} with four molecules per primitive cell, in which each chain has four antiparallel nearest neighbor chains related by inversion centers. Infrared and Raman spectra of pure crystalline HF and DF[62] and of isotopic mixtures HF/DF[63] were consistent with the inelastic neutron scattering spectrum[64] and suggested, on the basis of coincidence between Raman and ir lines in the stretching region, that the structure is D_{2h}^{17} with the primitive cell isomorphous with C_{2v}. Theoretical lattice dynamical analysis[62] indicated that the interchain force constants are 1/50–1/200 weaker than the intrachain hydrogen-bond force constant. Consequently, we treat the band structure in a single chain approximation with the C_{2v} structure (Fig. 2), although interchain forces could broaden the electronic bands in the solid.[1]

The minimum F–F distance established in x-ray studies is 2.49 ± 0.01 Å, and the angle α along the chain is 120.0°.[61] The hydrogen positions could not be anticipated from x-ray studies, although the Fourier projection obtained indicated an asymmetrical hydrogen bond (the H–F distance is shorter than one-half the F–F distance) statistically distributed between nearest fluorine atoms. The occurrence of such a structure is also supported by the absence of a residual zero-point entropy in solid HF.[65] Fluorine NMR studies[66] have suggested, from analysis of the second moment of the resonance line, an increase in the H–F distance in the solid relative to the isolated molecule bond length (R_{HF} 0.95 ± 0.03 Å in the solid vs 0.917 Å in the gas phase),[54] while the use of the empirical formula of Pimentel and McClelland[31] for intramolecular vs intermolecular bond length correlations (originally used for oxygen-hydrogen bonds) with $R_{FF} = 2.49$ Å reveals a molecular bond length $R_{HF} = 1.02$ Å in the solid. Since this increase in molecular bond length in the solid might have a significant effect on lattice force constants, cohesive energy, and atomic charges,[31–33] we treat solid HF with both its free-molecule HF distance and with the optimized bond length in the crystal.

Figure 3 shows the band structure of solid HF in the single chain approximation, the chain being oriented along the x axis with $R_{HF} = 0.92$ Å, $R_{FF} = 2.49$ Å, and an interchain angle of $\alpha = 180°$. Ten neighbors are considered in the lattice sums and 20 **K** points were used in the BZ sums. The self-consistency iterations are terminated when band energies and atomic charges in successive iterations agree within 10^{-5} a.u. and 10^{-4} e, respectively. Under these conditions, the energy bands are stable to within less than 0.001 eV. The one-electron energies of an isolated HF molecule with the same H–F distance are also indicated in the figure with the symmetry notation in the C_{2v} point group. This notation will be used for the corresponding crystal orbitals as well. Symmetry combinations of the molecular Bloch functions 2σ, 3σ, π, and 4σ, which belong to irreducible representations of the HF crystal in the linear chain approximation, were given by Bassani *et al.*[1] The band structure of the fictitious crystals $(H_2)_n$ and $(F_2)_n$, calculated with the same conformation, are also shown for comparison.

The energy shifts of the molecular eigenstates at the edges of the BZ due to crystal-field effects that were neglected in the non-self-consistent calculation of Bassani *et al.*[1] are shown to range from 2.38 eV for the lowest 2σ band, − 4.05 eV for the 3σ band, and − 2.42 eV for the unoccupied 4σ band, to a very small shift of − 0.04 eV for the π band. The degeneracy of the π level in the $C_{\infty v}$ group of the isolated HF molecule is not removed by the crystal field of the *linear* solid ($\alpha = 180°$). The crystal orbital $\psi_\pi(y, z)$ involves pure fluorine $2p_z$ and $2p_y$ orbitals and does not mix with other orbitals at any point of the BZ. Consequently, this band has a very small dispersion and crystal-field shift. The 2σ and 3σ bands are composed of fluorine $2s$, $2p_x$, and hydrogen $1s$ atomic orbitals. Owing to the substantial size these corresponding 2σ and 3σ molecular orbitals have in the free molecule along the axial direction,[67] the 2σ and 3σ bands also exhibit strong dispersion in **K** space. In the linear crystal case, the highest occupied state occurs at the center of the zone (Γ point) and is a 3σ band. The conduction state minimum also occurs at the center of the zone (at the 4σ band), and a very large (25 eV) direct energy gap is obtained. The ionization potential of the crystal is reduced by 1.4 eV relative to the isolated molecule ionization potential (20.1 eV for $R_{HF} = 0.92$ Å). The hydrogen bond formed in the crystal has a $1s$–$2s$

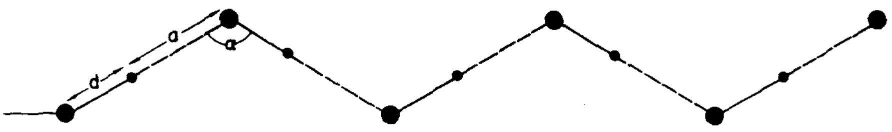

FIG. 2. Planar zigzag chain forming the crystal structure of solid HF. Intramolecular and nearest intermolecular distances are denoted by d and a, respectively. The chain angle is denoted by α.

bond order of 0.124 and a $1s-2p_x$ bond order of 0.165. The sublimation energy of the solid is calculated to be 12.1 kcal/mole, which is higher by 3.0 and 1.2 kcal/mole than the dimer and hexamer[17a] sublimation energies, respectively, calculated by the same method (Table II). The fluorine net atomic charge increases from $-0.275\, e$ in the free molecule to $-0.329\, e$ in the crystal. The significant changes in the one-electron energies, ionization potential, and charges in the solids reflect the strength of the hydrogen bond formed.

In passing from the $(F_2)_n$ and $(H_2)_n$ structures to the $(HF)_n$ structure, the $1\sigma_g$ band of the $(H_2)_n$ is stabilized, while the $2\sigma_g$ band of $(F_2)_n$ is destabilized in forming the $(HF)_n$ 2σ band. The doubly degenerated fluorine π band of $(F_2)_n$ is generally similar to the corresponding band in $(HF)_n$, the former having more pronounced dispersion due to the stronger $2p_\pi-2p_\pi$ interaction in the short F–F bond. When the total energy per molecule of these structures is optimized with respect to the chain angle α, both $(H_2)_n$ and $(F_2)_n$ have a minimum at $\alpha = 180° \pm 1°$, while the minimum for $(HF)_n$ occurs at $\alpha = 122° \pm 1°$, which is very close to the experimental value of $\alpha = 120°$. This is partly due to the more favorable F–F interaction in the zigzag HF structure, and mainly due to the stabilization effect of the next-nearest H–H interaction present in the hydrogen-bonded structure $(HF)_n$. The absence of this effect in both $(H_2)_n$ and $(F_2)_n$ structures suggests this is a hydrogen-bond effect. The $E_{tot}(\alpha)$ curve for solid HF is extremely flat, as was also observed in similar calculations of HF dimers.[17a,17b,18,58] The stabilization energy gained by bending the chain is only 0.2 kcal/mole.

Several modifications occur in the band structure upon bending the linear chain. In the zigzag structure, there are two molecules in the unit cell. The degeneracy of the $\pi(y,z)$ band is removed to yield two $\pi(y)$ and two $\pi(z)$ bands. The former bands now interact with the σ manifold, while the $\pi(z)$ bands, belonging to the Γ_2 representation (notation of Ref. 1), do not mix with any other bands and have a low dispersion. The highest occupied valence band is now the $\pi(y)$ band, while the 3σ band that formed the top of the valence band in the linear case is lowered. The lowest state in the conduction band remains at the zone center and the band gap

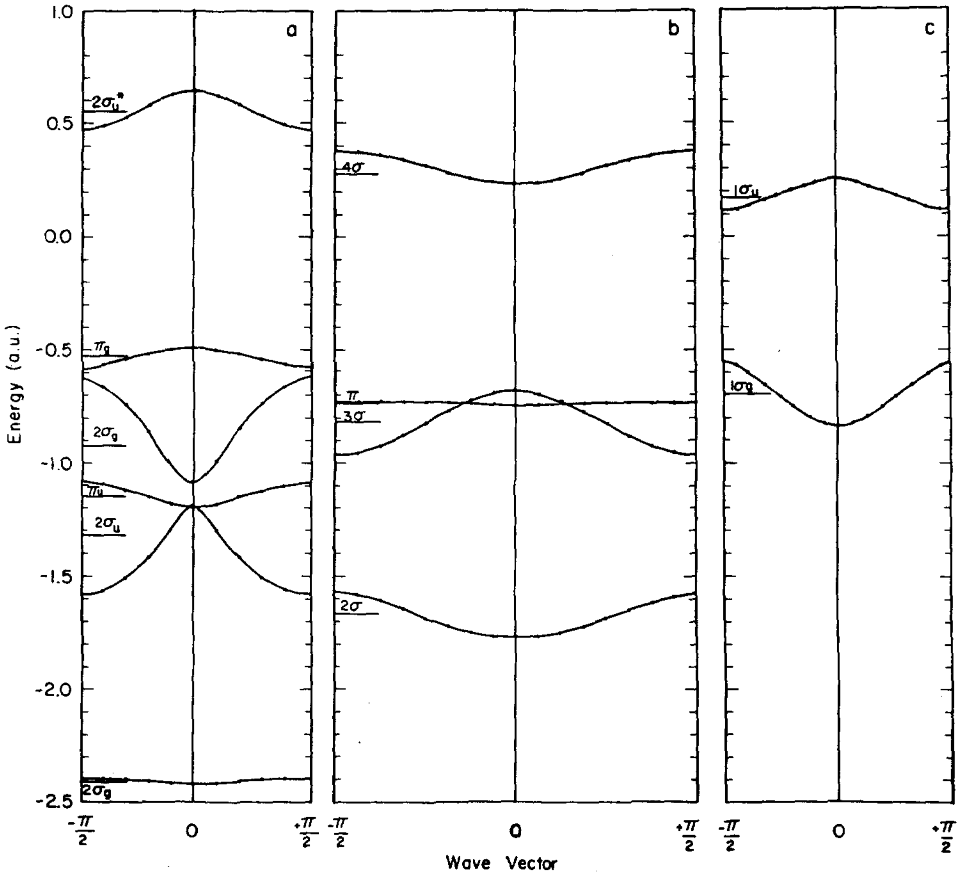

FIG. 3. Band structure of (a), $(F_2)_n$; (b), $(HF)_n$; and (c), $(H_2)_n$ with $a = 1.57$ Å, $d = 0.92$ Å, and $\alpha = 180°$. Twenty K-grid points and 10 orders of interaction were used. The band structure was iterated to full self-consistency. The energy of the corresponding levels in the isolated molecule with the same d value and their point group representation notations are indicated.

decreases to 22.5 eV. The crystal ionization potential is reduced by 2.2 eV relative to the ionization potential of the isolated HF molecule having the same bond length R_{HF}. A much smaller lowering of the ionization potential (0.7 eV) was obtained by Bassani *et al.*,[1] owing to the neglect of crystal field effects.

The Davydov splitting in the 4σ band is 4.1 eV and is characteristic of strong intermolecular coupling. The charge distribution and the hydrogen-bond order are almost unchanged relative to the linear case. Owing to the very small stabilization gained by bending the HF chain, we now proceed to examine the convergence effects on the band structure by considering the linear structure.

B. Convergence effects

We start with the convergence of the band structure and charges as a function of the K grid used in Eqs. (9) and (10). After taking an interaction radius which corresponds to 1 order of interaction and interating the energy eigenvalue problem to full self-consistency, the band structure is evaluated for increasing cluster sizes, each time adding to the sum additional K points evenly spread in the BZ. It should be noted that the method used here to evaluate the band structure is a real-space technique rather than a reciprocal-space representation like the tight-binding, APW, OPW, and Korringa–Khan–Rostoker (KKR) methods in which the crystal wavefunction is chosen to be explicitly wave vector dependent by imposing translational invariance on it. Consequently, the inclusion of a given K grid in our calculation via Eq. (9) is obtained by increasing the number of atoms in the cell, keeping the interaction radius constant. The results of this convergence check are shown in Table III. It is evident that at least six to ten evenly spread K points are required to obtain stability of the bands and charges within 10^{-4} a.u. and $10^{-4}e$, respectively. The $\pi(y,z)$ band, which is less dispersed in K space and has no direct interaction with other bands, converges most rapidly; while more disperse bands, like the 2σ, are changed more pronouncedly by using a higher mesh K grid. Similarly, the Hartree–Fock matrix elements of the orbitals that are relatively localized in real space ($2s$ orbitals) are changed to a smaller extent than elements coupling orbitals that are more extended (like the $2p$ orbitals). The cohesive energy changes by as much as 14% in the fully convergent result, reflecting the net stabilization of all occupied bands due to the increase in the K grid mesh. Similar results were also obtained when the interaction range was extended to include 3 orders of neighbors, except that in this case only results corresponding to at least seven grid points can be obtained and some of the characteristics of the behavior at low mesh grid are lost.

In other self-consistent calculations on ionic-covalent solids,[41] it was found that when only a few high symmetry points in the BZ are used relatively poor results are obtained,[39a] since high-symmetry points are usually a poor representation of the totality of the BZ points unless a large density of states is accumulated around them. This can be demonstrated in HF by considering the $\mathbf{K}_p$-grid dependence of the charge-bond matrix in Eq. (9). Its diagonal elements correspond to the atomic orbital charge contributed by all occupied bands in the ground state:

$$P_{\mu s,\mu s} \equiv Q_{\mu s} = \sum_{\mathbf{K}_p} \sum_{\gamma=1}^{\sigma_{\mathrm{occ}}} 2c^{*}_{\mu s\gamma}(\mathbf{K}_p) C_{\mu s\gamma}(\mathbf{K}_p) = \sum_{\mathbf{K}_p} Q_{\mu s}(\mathbf{K}_p). \qquad (12)$$

The fraction of orbital charge contributed by all occupied bands at a selected limited grid $\{\mathbf{K}_p\}$ is denoted by

$$f_{\mu,s}(\{\mathbf{K}'_p\}) = \sum_{\mathbf{K}_p \in \{\mathbf{K}'_p\}} Q_{\mu s}(\mathbf{K}_p)/Q_{\mu s}. \qquad (13)$$

Calculating, for instance, the $2s$ orbital charges on a given fluorine atom considering only zone-center ($\mathbf{K}=0$) contributions yields a value of 0.0593 for f. Addition of zone-edge contributions increases it to 0.1795, while sampling of ten evenly spaced points (including zone edge and zone center) increases it to 0.8342. Similar results are obtained for the other orbital charges. Since the dispersion of the $Q_{\mu s}(\mathbf{K}_p)$ charges is relatively large, sampling of evenly spaced $\mathbf{K}_p$ points is inevitable. In the SPC method, the K points appearing in the calculation are always evenly spread in the BZ, thereby generating a better representation of the charges and one-electron energies. Similar large discrepancies in the band structure calculations were indicated by Drost and Fry[39a] in computing the bands of LiF with both a few symmetry K points and 89 evenly distributed K points.

TABLE III. Convergence of band energies at K = 0, Hartree–Fock matrix elements from the final SCF iteration, cohesive energy and net atomic charge as a function of the number of K-grid points. One order of interaction and converged SCF interations are employed.

Number of nonequivalent points	$E_{2\sigma}$ (K = 0) (a.u.)	$E_{3\sigma}$ (K = 0) (a.u.)	$E_{\pi}(yz)$ (K = 0) (a.u.)	$E_{4\sigma}$ (K = 0) (a.u.)	ΔE (kcal/mole)	$Q_{\mathrm{F}}^{\mathrm{net}}$ (e)	$F_{2s,2s}$ (a.u.)	$F_{2px,2px}$ (a.u.)	$F_{2py,2py}$ (a.u.)
3	−1.7601	−0.6881	−0.7430	+0.2391	9.73	−0.3312	−1.4772	−0.5215	−0.7400
4	−1.7643	−0.6872	−0.7432	+0.2364	10.24	−0.3281	−1.4773	−0.5210	−0.7407
6	−1.7675	−0.6851	−0.7436	+0.2321	10.91	−0.3231	−1.4775	−0.5205	−0.7409
8	−1.7676	−0.6850	−0.7438	+0.2320	10.99	−0.3229	−1.4777	−0.5204	−0.7410
10	−1.7677	−0.6849	−0.7438	+0.2319	11.12	−0.3227	−1.4778	−0.5203	−0.7410
16	−1.7677	−0.6848	−0.7438	+0.2317	11.31	−0.3227	−1.4778	−0.5203	−0.7411
20	−1.7677	−0.6848	−0.7438	+0.2317	11.32	−0.3227	−1.4778	−0.5203	−0.7411

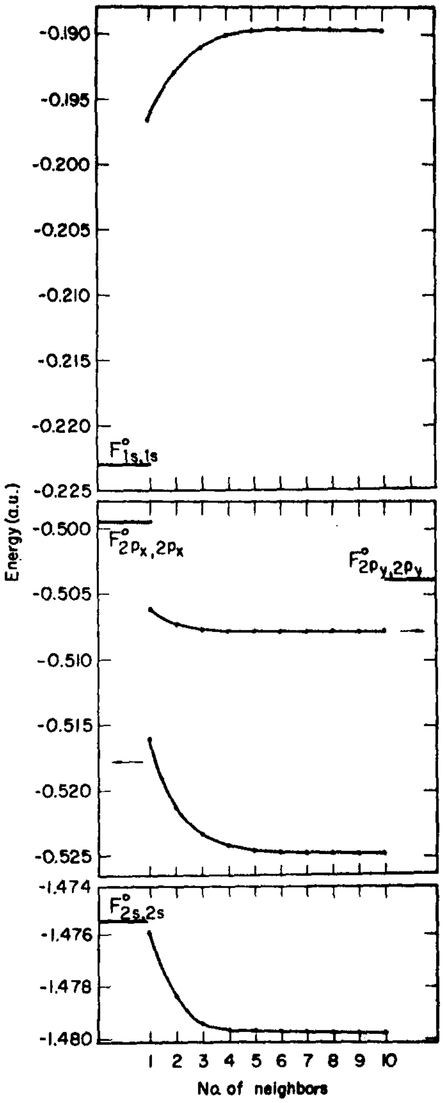

FIG. 4. Dependence of the final Hartree–Fock diagonal matrix elements on the interaction order, $a = 1.57$ Å, $d = 0.92$ Å, and $\alpha = 180°$. The K sun and the SCF interaction cycles are convergent. The value of the corresponding elements in the isolated HF molecule with $d = 0.92$ Å are indicated.

We next examine the interaction radius convergence problem. The band structure is now calculated for the largest cluster $(HF)_{20}$ employing 20 evenly distributed K points in the calculation of the charge matrix. The energy eigenvalue equations are iterated to full self-consistency and the interaction radius is increased from 1 order up to 10 orders (23.3 Å).

The various diagonal elements of the final Hartree–Fock matrix in the atomic orbital representation for increasing interaction orders is shown in Fig. 4. On the side of each figure, the corresponding elements calculated from the final Hartree–Fock matrix of the isolated HF molecule having the same internuclear distance are indicated.

The fluorine $(2s, 2s)$ element is stabilized by the crystalline environment only to a small extent, behaving approximately as an unpolarized core state. The $(2p_y, 2p_y)$ element, which is degenerate with the $(2p_z, 2p_z)$ element, is likewise only weakly stabilized, since the $2p_y$ orbitals are perpendicular to the chain axis and interact only weakly with the rest of the orbitals. On the other hand, the fluorine $(2p_x, 2p_x)$ element is markedly decreased owing to the strong interaction of the fluorine $2p_x$ manifold along the chain axis. The matrix elements involving fluorine orbitals are all stabilized in the crystal, since the F atoms gain electronic charge relative to the isolated molecule state. The hydrogen $(1s, 1s)$ elements are destabilized, since the charge is donated by these orbitals in the crystal. The largest change in energy in the elements experiencing strong modification in the crystal occurs just after the first order of interaction is introduced. A further increase in interaction radius has a less pronounced effect which tends to level off at around four–five interacting neighbors, with a net maximal change of 0.7 eV. In the nonlinear chain, the degeneracy of the $(2p_y, 2p_y)$ and $(2p_z, 2p_z)$ elements is removed, the resulting matrix elements of the $2p_y$ orbitals now exhibiting a stronger shift from the energy value corresponding to the free molecule, due to interaction with the $2s$ orbitals. It should be noted that in the LCAO scheme used, unoptimized atomic orbitals are employed. The use of fully optimized SCF orbitals would have increased the convergence rate obtained here, owing to the smaller extension of the molecular charge along the bond direction.

Figure 5 shows the dependence of band energies at K = 0 on the interaction order. It is evident that the low energy 2σ band that is separate from other bands converges rapidly, while the other bands exhibit a slower convergence. Generally, 4–5 orders of interaction are sufficient to obtain bands that are stable to within 10^{-4} a.u. The convergence of the cohesive energy and atomic

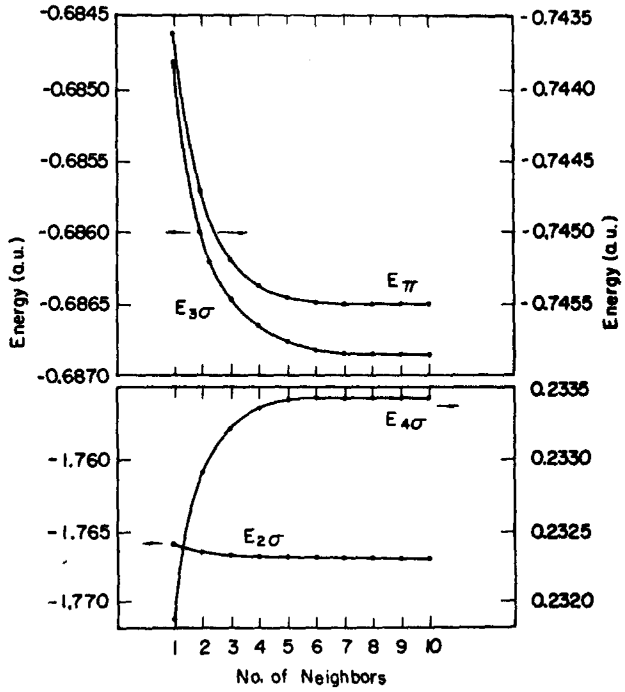

FIG. 5. Dependence of the band energies of $K = 0$ on the interaction radius, $a = 1.57$ Å, $d = 0.92$ Å, and $\alpha = 180°$. The K sum and the SCF iteration cycle are convergent.

charge is shown in Figs. 6a and 6b, respectively. Four to five neighbors are sufficient to obtain the cohesive energy to within less than 0.1 kcal/mole from the convergence limit result. The fluorine charge in the crystal is also compared with the corresponding value for the isolated HF molecule in Fig. 6b. It is again demonstrated that the charge redistribution in the hydrogen-bonded solid is significant (here the change in the net charge amounts to 17%) and that the isolated molecule charge distribution should not be used in band structure calculations for such solids.[1]

The effect of increasing the number of interacting units on the charge redistribution accompanying the intermolecular hydrogen-bond formation may be demonstrated by comparing "difference potential" maps of clusters of increasing size. Thus, the difference between the electrostatic potential generated by superimposing n free-molecule charge densities and that generated by the charge density of a $(HF)_n$ structure is investigated for several n values. An open nonperiodic chain is used for simplicity. We utilize the method suggested by Srebrenik *et al.*[68] for the analytical solution of the Poisson equation for charge density that can be expressed in terms of Gaussians. The charge density $\rho(\mathbf{r}_1)$ obtained from the solution of the N-electron Schrödinger equation is given by

$$\rho(\mathbf{r}_1)=\int \Psi^*(\mathbf{r}_1\mathbf{r}_2\cdots\mathbf{r}_N)\Psi^*(\mathbf{r}_1\mathbf{r}_2\cdots\mathbf{r}_N)\,d\tau\cdots d\tau_N\,. \tag{14}$$

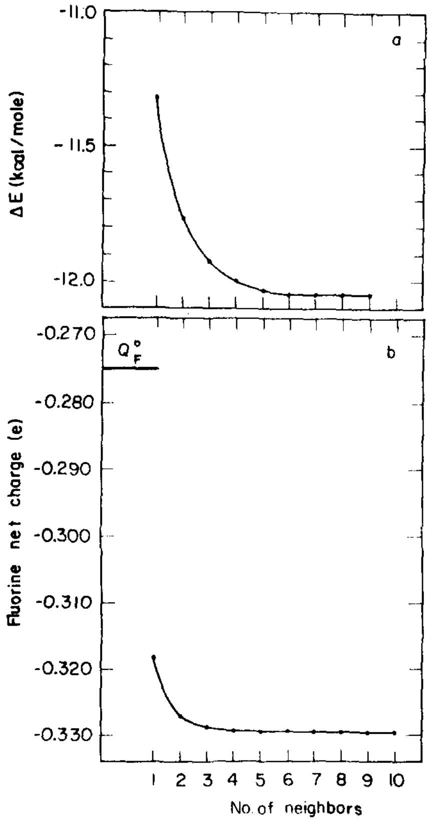

FIG. 6. Dependence of the cohesive energy per molecule (a) and the fluorine net charge (b) on the interaction order. Q_F^0 indicates the fluorine net charge in the isolated HF molecule with $d=0.92$ Å.

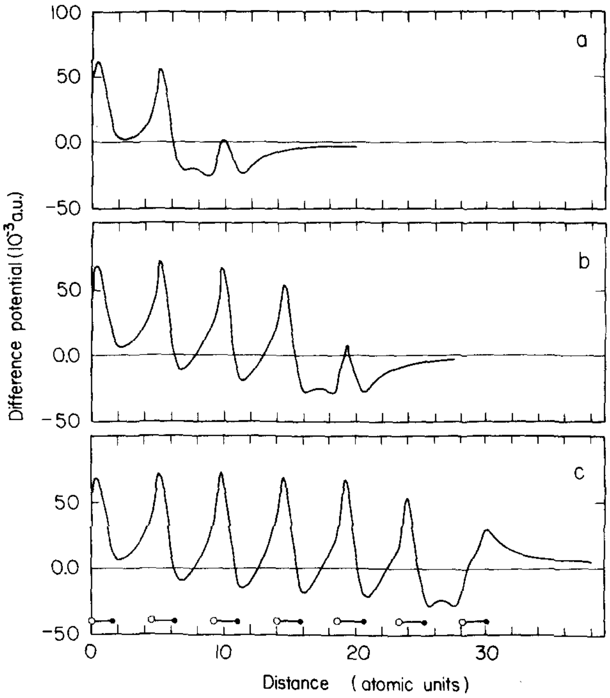

FIG. 7. The difference in electrostatic Poisson potential between a linear $(HF)_n$ chain ($a=1.57$ Å, $d=0.92$ Å, $\alpha=180°$) and a superposition of n unperturbed isolated molecule potentials with the same geometry. (a), $(HF)_3$; (b), $(HF)_5$; (c), the end segment of $(HF)_{20}$.

The Poisson electronic potential generated by this charge distribution is obtained from

$$\nabla^2 V_{\text{elec}}(\mathbf{r})=4\pi\rho(\mathbf{r}) \tag{15}$$

and represents an electrostatic potential incorporating the quantum effects through the derivation of Ψ. The total potential is obtained by adding the nuclear potentials

$$V_{\text{nuc}}(\mathbf{r})=\sum_n \frac{Z_n}{|\mathbf{R}_n-\mathbf{r}|} \tag{16}$$

to $V_{\text{elec}}(\mathbf{r})$. The Slater orbitals used by us as basis functions can be easily expanded into Gaussians using the 6-G expansion given by Hehre *et al.*[69] It has previously been shown that potentials derived from INDO wavefunctions yield very good agreement with potentials generated from *ab initio* wavefunctions[70] by numerical intergration. Since population analysis oversimplifies the charge redistribution, and simple charge-density maps are not sensitive enough to these effects,[71] potential maps provide a much better indication of actual rearrangements occurring upon intermolecular bond formation.

Figure 7 represents the difference potential for clusters with $n=3, 5, 20$. In the latter case, only the last seven HF units are displayed. It is evident that upon hydrogen-bond formation the H atom loses electronic charge and has a lower electrostatic potential, whereas the potential at the fluorine atom increases. Most of the intramolecular HF region manifests a buildup in potential; while close to the hydrogen atom the potential decreases, reaching a minimum in the intermolecular region. A similar calculation on the $(HF)_5$ fragment [Fig. 7 (b)] shows that the potential differences are markedly changed at the end F–H$\cdots$F segment from those in the corresponding $(HF)_{20}$ case, indicating that charge rearrangement in the A–H$\cdots$B moiety depends also on more distant atoms in the structure. Thus, models that consider only A–H, B–H, and A–B interactions[19, 20] are inadequate for a realistic description of phenomena in such $(A\text{–}H\text{–}B)_n$ hydrogen-bonded systems. Similar conclusions were suggested by Morakuma and Peterson[72] and by Kollman and Allen.[73] The redistribution effects manifested by the HF chain are qualitatively similar to those calculated by Kollman and Allen[17b] from their HF-dimer charge-difference maps, although edge effects are probably very marked in their highly truncated $(HF)_2$ system.

Tight-binding calculations[1] that generate the crystal potential from direct superpositions of unperturbed free-molecule charge densities completely neglect the potential rearrangement effects shown in Fig. 7 and probably cause a severe underestimation of binding effects, band dispersion, and crystal-field shift. It should be mentioned that the linear superposition approximation is probably a better one in the band structure calculation of van der Waals solids, such as CH_4,[74] where similar difference potential calculations have indicated very shallow and flat potential differences.

We now turn our attention to the third convergence problem, namely the convergence of the self-consistent cycle. In previously reported[39a, 40, 41] self-consistent band structure calculations for atomic crystals, the crystal potential at any point in the unit cell is self-consistently adjusted on the basis of the recalculated band functions. In molecular crystal calculations,[1, 74] usually only the intramolecular potential is taken to be self-consistent (using self-consistent free-molecule electrostatic potentials), while intermolecular interactions are treated in a non-self-consistent tight-binding model. Electrostatic potential redistribution effects in the intermolecular region (Fig. 7) suggest that this might be a poor approximation for hydrogen-bonded solids in view of the large polarization effects in this region.

TABLE IV. Values of diagonal Hartree–Fock energy matrix elements, band energies (at K=0), charges and cohesive energy for different self-consistency (SC) requirements. Full SC indicates that both intra- and intermolecular potentials are self-consistently adjusted.

Property	Full SC (12 iterations)	Intramolecular SC	Full SC (1 iteration)
Diagonal elements (a.u.)			
$F^{(H)}_{1s,1s}$	−0.1899	−0.2230	−0.1982
$F^{(F)}_{2s,2s}$	−1.4798	−1.4776	−1.4709
$F^{(F)}_{2p_x,2p_x}$	−0.5247	−0.4939	−0.5305
$F^{(F)}_{2p_y,2p_y}$	−0.7428	−0.7387	−0.7408
Band energies at $K=0$(a.u.)			
$E_{2\sigma}$	−1.7692	−1.7712	−1.7682
$E_{3\sigma}$	−0.6868	−0.6771	−0.6816
E_{π}	−0.7455	−0.7414	−0.7449
$E_{4\sigma}$	0.2336	0.2257	0.2277
Partial charges (e)			
Q^{F}_{2s}	−1.8710	−1.8728	−1.8646
$Q^{F}_{2p_x}$	−1.4585	−1.4054	−1.4735
$Q^{F}_{net}=-Q^{H}_{net}$	−0.3235	−0.2752	−0.3381
Cohesive energy (kcal/mole)	12.1	9.4	9.7

Band energies at the zone center, diagonal Hartree–Fock energy matrix elements, partial charges, and the cohesive energy, calculated with self-consistent adjustment of both intra- and intermolecular potentials up to the convergence limit, are compared in Table IV with the results obtained by the method of Bassani *et al*,[1] where only the intramolecular elements are self-consistently refined. It should be noted that the true molecular anisotropy is retained in both our calculations, while in that of Bassani *et al.* the potential was spherically averaged around each atom. In each case, 20 K grid points were used and 10 orders of interactions were retained.

Diagonal Hartree–Fock elements are shown to deviate significantly in the calculation, when only intramolecular self-consistency is retained. The smallest deviation occurs in the $2s$ elements (0.06 eV) which roughly represent core elements, and in the $2p_y$ elements (0.1 eV) which represent the energy of orbitals perpendicular to the chain axis. Other elements exhibit a more pronounced change (0.8–0.9 eV for the $1s$ and $2p_x$ elements) resulting in deviations of the order of 0.2–0.3 eV in the band energies. The net charge is somewhat low in the calculation retaining only intramolecular self-consistency mainly owing to the underestimation of the charge transferred by the $2p_x$ orbitals along the hydrogen-bond direction. The cohesive energy is also shown to be grossly underestimated by this approximation.

Treating both intra- and intramolecular self-consistency on the same level, we observe (Table IV, Col. 4) that even one iteration results in somewhat better agreement with the fully convergent results, although the bands are still not fully stabilized and the cohesive energy is small.

Owing to the relatively rapid convergence of the K sums, of the interaction radius dependent energies, and of the self-consistent cycle, it is possible to treat various structural optimization problems such as conformation, stability, and relaxation of the lattice around point defects with moderate computer time. In the following calculations we consider the fully convergent SCF results with 6 orders of interactions and 10 K points. Such a calculation requires 1.3 min on a CDC 6600 computer.

C. Truncated-crystal models

Due to the nonadditivity of bond energies and the strong edge effects manifested by HF dimers and trimers, the electronic and structural properties of the

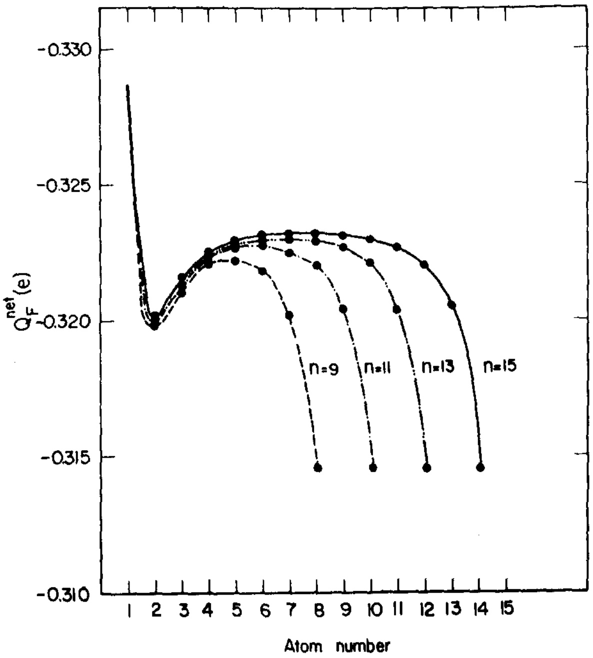

FIG. 8. Fluorine net atomic charges as a function of position along the nonperiodic $(HF)_n$ chain for $n = 9$, 11, 13, and 15. Experimental structure ($a = 1.57$ Å, $d = 0.92$ Å, and $\alpha = 120°$) is assumed.

F–H···F bond in crystals and polymers have previously been investigated on truncated-crystal models using $(HF)_6$ clusters[16, 18, 24] and $(HF)_8$ clusters.[17a] The validity of the truncated-crystal model for hydrogen-bonded chains is examined by performing INDO calculations on $(HF)_n$ chains having the experimental crystal conformation ($R_{FF} = 2.49$ Å, $\alpha = 120°$, and R_{HF} assumed 0.92 Å) and comparing the results with those obtained in band structure calculations for periodic structures. The chain length examined extends up to 20 HF units.

The fluorine net atomic charge for atoms labeled 1–15 in chains with increasing length are plotted in Fig. 8. It is evident that for small chains ($n \leq 9$) the number of atoms experiencing a "bulk" atomic charge is small compared with the total number of chain atoms and that edge effects propagate quite deeply into the "bulk". Only for $n = 15$ do the three interior fluorine atoms have approximately equal charges. Taking this cluster size, we examine the effect of charge inhomogeneity on the Hartree–Fock matrix elements in Fig. 9. Likewise, it is seen that only the central atoms exhibit an approximate constancy in these elements. Thus, edge effects propagate some six to seven molecular units into the bulk of the chains, as far as charges and energy matrix elements are concerned.

The convergence behavior of the fluorine atomic charge of the innermost atom in each cluster and the energy per molecule as a function of cluster size are shown in Fig. 10. Owing to inhomogeneity effects, the values of band energies even in the largest cluster considered $[(HF)_{20}]$ still deviate significantly from the results obtained in a similar calculation using a periodic structure. The ionization potential for $(HF)_{20}$ is off by 1.2 eV from the periodic cluster value, the bandgap is overestimated by 2.5 eV, and the valence band is wider by 1.8 eV. The atomic charge of the central atom in the cluster (Fig. 10), on the other hand, converges reasonably, 5–7 orders of interaction being sufficient to assure its stability.

Another demonstration of edge effects in such truncated-crystal models is shown in Fig. 7, where potential difference functions are computed for chains of varying size. The electrostatic potential differences at the edges are seen to differ markedly from the chain center potentials, and only several HF units in from the edge are these perturbations damped. These penetration effects also indicate that surface states and point defect structures in hydrogen-bonded chains are not amenable to the band-edge treatments suggested by Levine[75] and Davison and Koutecky,[76] in which the defect perturbative effect is assumed to be localized on a single atom. It is thus concluded that results of truncated-

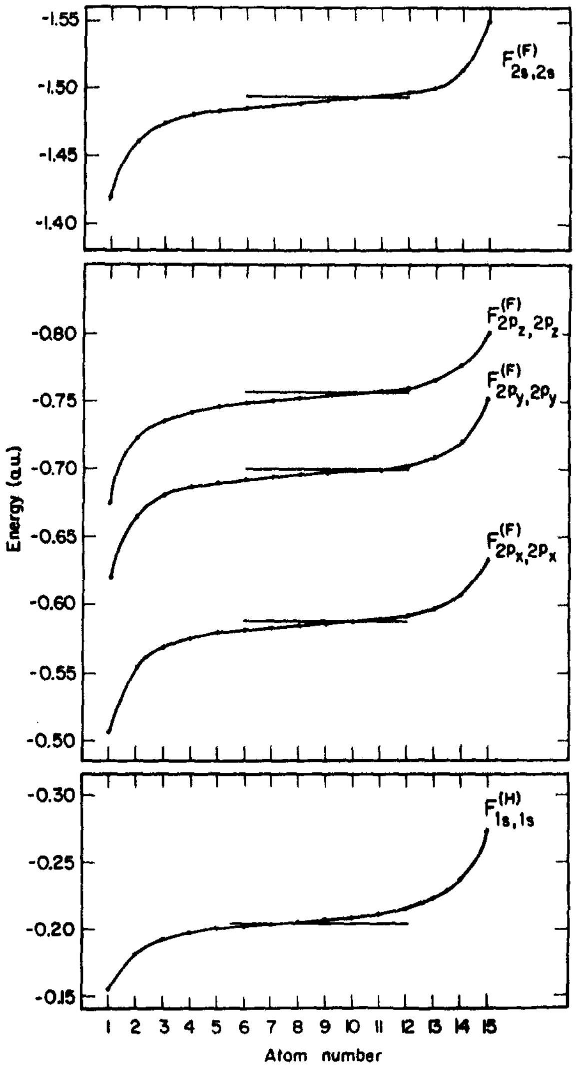

FIG. 9. Diagonal Hartree–Fock energy elements for the truncated $(HF)_{15}$ chain as a function of the position of the atoms. Horizontal lines denote the corresponding $F^0_{\mu,\mu}$ element in the crystal, as obtained in the convergence limit of SPC calculations. The experimental structure with $a = 1.57$ Å, $d = 0.92$ Å, and $\alpha = 120°$ is assumed.

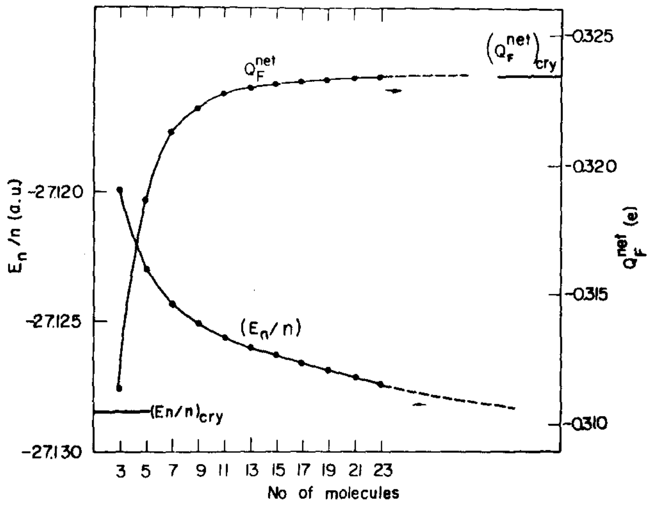

FIG. 10. Dependence of the energy per molecule (E_n/n) and the net atomic charge (Q_F^{net}) of the central fluorine atom on the number of molecules in the truncated crystal. Experimental structure assumed. $(E_n/n)_{cry}$ and $(Q_F^{net})_{cry}$ indicate the values corresponding to a periodic structure with the same geometry.

crystal calculations employing a small number of hydrogen-bonded units ($n < 15$) should be applied with great caution to the examination of energetic and charge-dependent properties of the corresponding infinite periodic structure.

IV. STRUCTURE OPTIMIZATION

The small-periodic-cluster method, utilizing a self-consistent LCAO representation of the crystal orbitals, is capable of treating variations in unit cell structure and dimensions which differ from the experimental equilibrium values, without further assumptions on hybridization or interaction matrix elements needed in empirically adjusted pseudopotential[77a] or tight-binding[77b] methods or interpolation schemes[78] for band structure calculations. Owing to the explicit use of a self-consistent scheme based on atomic rather than molecular[1] or crystal data,[77,78] one can examine the stability of a given crystal structure against changes in unit cell dimensions or translations and rotations of molecules inside the unit cell, thereby maintaining the theoretical equilibrium geometry. Since, in constructing the wavefunctions in the SPC method, we did not use the space symmetry of the crystal to factorize the secular equations, it is possible to investigate within this scheme the energy associated with lattice distortions that do not preserve the symmetry of the primitive unit cell, such as those accompanying lattice mode vibrations. Thus, for a given distortion (e.g., symmetric stretching of the fluorine sublattice), we obtain the total crystal energy as a function of the distortion coordinates. This permits the calculation of force constants for various lattice vibrations. Such a calculation is very difficult to implement by band structure methods that employ symmetry-adapted wavefunctions explicitly.

For minimizing the total energy, we employ the steepest-descent method, in which the displacement $\delta\xi$ in the vector ξ required to approach static equilibrium is iteratively determined by

$$\delta\xi = -G\nabla_\xi E_{\text{tot}}(\xi) , \qquad (17)$$

where $E_{\text{tot}}(\xi)$ denotes the total Hartree–Fock energy [Eqs. (11a) and (11b)] of a crystal with structure parameters given by the components of ξ, and G is a scaling factor. The required derivatives are numerically calculated from the total energy of a crystal where 10 K-grid points and six neighboring interactions are considered. Near the minimum, the first derivative method is nonconvergent and a simple mapping procedure is used. Differences in successive iterations of the order of 0.002 Å and 1° in distance and angles, respectively, are taken as convergence criteria.

We first consider the optimization problems for the linear structure with $\alpha = 180°$. We start with the experimentally obtained F–F distance $(a+d) = 2.49$ Å. Minimization of the total energy yields a fully planar structure with a $a = 1.475$ Å and $d = 1.015$ Å. This amounts to an increase of 0.009 Å in the intramolecular H–F bond relative to the free molecule value obtained by the INDO method. The cohesive energy is 17.8 kcal/mole. A structure with $(a+d) = 2.49$ Å, but with $d = 1.006$ Å corresponding to the HF bond length predicted by the INDO method for the isolated molecule, reveals a cohesive energy of 17.1 kcal/mole, indicating that the intramolecular bond rearrangement further stabilizes the hydrogen-bonded structure. The fluorine net atomic charge undergoes a significant modification upon formation and stabilization of the bond, becoming $-0.345\ e$ compared with $-0.268\ e$ in the equilibrium configuration of an isolated molecule. This compares favorably with the values of $-0.327\ e$ and $-0.225\ e$ obtained by Del-Bene and Pople[16] for the monomer and hexamer, respectively, by the minimal basis set *ab initio* method. Formation of the hydrogen bond with $(a+d) = 2.49$ Å, without relaxing the intramolecular bond length, lowers the free molecule net charge by 16%, and a further lowering by 6.2% accompanies the intramolecular bond rearrangement in the crystal. It should be noted that such effects are completely neglected by theories that use a phenomenological nonbonded atom–atom or bond–bond potentials to compute the crystal conformation[21–24] under the rigid molecule approximation. Similarly, the transferability of the atomic charges of the isolated molecule to the molecular crystals, for computing electrostatic interactions in the hydrogen-bonded system,[24] seems questionable in view of the significant modifications the charges undergo in the solid due to charge transfer and intramolecular relaxation.

Optimization of the crystal structure, subject to the condition that the intramolecular bond length d remains unchanged relative to the isolated molecule equilibrium state revealed by the INDO method, results in $a = 1.22$ Å $(a+d = 2.226$ Å) and a cohesive energy ΔE of 22.2 kcal/mole. A similar optimization performed by Del-Bene and Pople[16] on the hexamer by the *ab initio* method revealed a structure with $(a+d) = 2.2$ Å but with a much lower cohesive energy of 12.7 kcal/mole. This is in line with the tendency of the INDO method (see Table II) to overestimate the intermolecular binding energies significantly.

A full optimization of the structure relative to all the out-of-plane angles of the molecules in the crystal and a, α, and d independently, reveals at equilibrium a fully planar structure with $a=d=1.125$ Å, $\alpha=122°$, and $\Delta E=29.5$ kcal/mole. In view of the strong tendency of the INDO method to underestimate the intermolecular bond length and to overestimate the intermolecular cohesive energies, it seems that the results of the full optimization are unlikely to be correct and that attention should be focused on the trends obtained, rather than on the absolute configuration deduced. Nevertheless, it is instructive to observe the effects introduced by polarization and charge transfer on the equilibrium geometry and charge distribution in the solid. For this purpose, we calculate the cohesive energy in the following three approximations:

(a) First-order perturbation theory using the isolated HF molecule wavefunction as zero-order vectors to yield the stabilization energy $E^{(1)}$;

(b) SCF theory for the periodic structure with intramolecular bond length fixed at the isolated molecule value. The stabilization energy is denoted E_{SCF};

(c) SCF theory for the periodic structure with optimization of the intramolecular bond length at each intermolecular separation. The stabilization energy is denoted $E_{\mathrm{SCF}}^{\mathrm{rel}}$, and the optimization procedure indicated in Eq. 15 is used where ξ now indicates the intramolecular bond lengths.

The difference $E_{\mathrm{SCF}}-E^{(1)}$ denotes the contribution of charge transfer and polarization[15] (sometimes referred to as delocalization energy) to the total stabilization energy. Figure 11 reveals the dependence of $E^{(1)}$, E_{SCF}, and $E_{\mathrm{SCF}}^{\mathrm{rel}}$ on the intermolecular distance a.

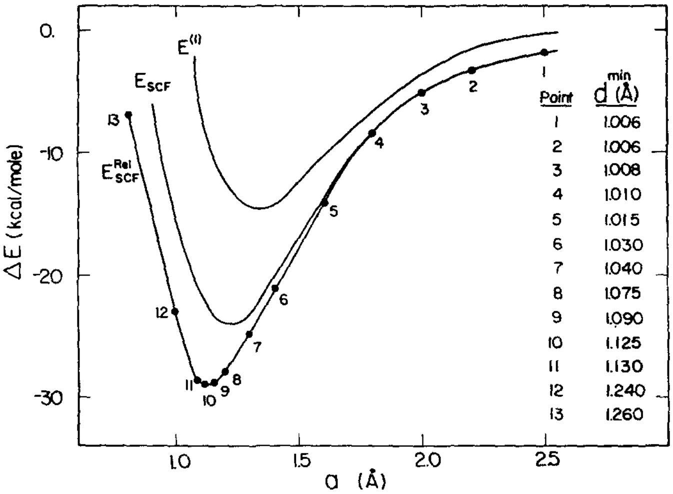

FIG. 11. Contributions of $E^{(1)}$, the first-order interaction energy E_{SCF}, the full SCF energy in the rigid-molecule approximation, and $E_{\mathrm{SCF}}^{\mathrm{rel}}$, the SCF energy with optimization of the intramolecular bond, to the crystal cohesion. The numbering on the curve $E_{\mathrm{SCF}}^{\mathrm{rel}}$ refers to the value of the optimized intramolecular bond length given in the insert.

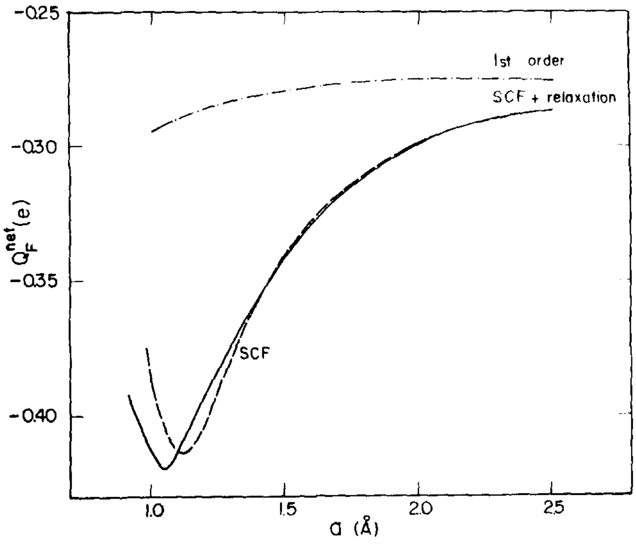

FIG. 12. Fluorine net atomic charge as a function of intermolecular separation, calculated by first-order theory, SCF with rigid molecules, and SCF with relaxation of the intramolecular bond length.

The first-order energy $E^{(1)}$ shows a minimum at $a=1.33$ Å with $\Delta E=12.2$ kcal/mole. Charge transfer and polarization increase the stabilization energy to 22.2 kcal/mole and shift the minimum to 1.22 Å. Relaxation of the intramolecular bond length further stabilizes the energy to 29.5 kcal/mole, shifting the minimum to $a=1.125$ Å ($R_{\mathrm{FF}}=2.25$ Å). Polarization and charge-transfer effects begin to be apparent at relatively long intermolecular separations ($a\sim 3.3$ Å), while the effects introduced by relaxation are apparent only at distances shorter than $a=1.8$ Å. The long-range effects introduced by the distortion of the molecular charge density in the solid were argued[15] to arise from the direct Coulomb energy, while the exchange contributes to the charge transfer and polarization affects the energy only at relatively short distances.

The fluorine net charge calculated from the first-order treatment, the SCF procedure with rigid intramolecular bonds, and the SCF procedure with the fully relaxed conformation are compared in Fig. 12. It is evident that a first-order treatment allows only for a very small modification of molecular charges in the solid (brought about by the antisymmetrization of the unperturbed wavefunctions due to intermolecular exchange), while an SCF treatment drastically changes the molecular charges in the solid, yielding thereby a much stabilized system. Relaxation of the intramolecular bond length introduces further adjustments in the atomic charges, minimizing the interpenetration of the charge clouds and thus decreasing the repulsive forces at short distances.

We next consider the variation in potential energy of a HF lattice as a function of the collective proton displacements coordinate $R=R_{\mathrm{FF}}/2-R_{\mathrm{HF}}$, for several R_{FF} distances. The results are shown in Fig. 13. For all R_{FF} distances considered, the crystal structure corresponding to minimum energy is planar, in accord

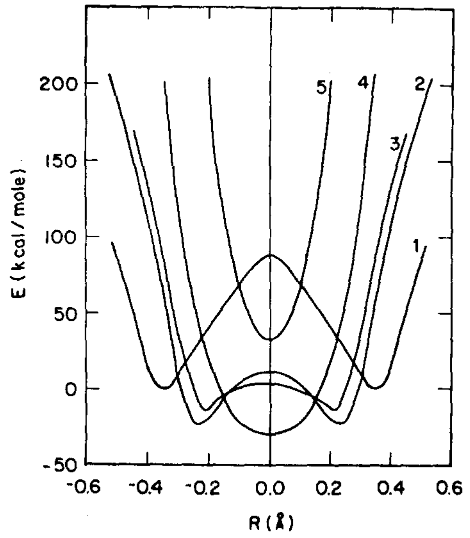

FIG. 13. Potential energy for collective proton displacement $R=(\frac{1}{2}R_{FF}-R_{HF})$ for a fixed fluorine sublattice with various R_{FF} distances: $R_{FF}=$ (1) 2.73 Å, (2) 2.49 Å, (3) 2.40 Å, (4) 2.25 Å, (5) 2.00 Å.

with the results of Del-Bene and Pople[16] for the hexamer. It is observed that for large R_{FF} values, a double minimum is obtained with a barrier which decreases with decreasing R_{FF} value. For small R_{FF} distances, a single well is obtained whose stabilization is lowered when the R_{FF} distance is further decreased. At the vicinity of the double well–single well transition, the potential for proton movement becomes flat and the protons exhibit strong delocalization. At the R_{FF} range where a double well persists, the protons of the crystal could be viewed as collectively resonating between the two equivalent asymmetric positions and should reveal a statistical proton density distribution. Such a distribution is observed in the crystallographic Fourier projection, obtained in x-ray diffraction.[61]

The double well potential for the collective displacement of the protons in HF is characterized by a high barrier (22.6 kcal/mole for symmetrical displacement), suggesting that macroscopic changes in the polarization should not be observing up to the melting point (at $kT=0.38$ kcal). Contrary to other hydrogen halides, the HF crystal does not exhibit any phase transition (judging by the heat capacity measurements,[65] as dielectric relaxation has not been measured) up to the melting point, due to strong hydrogen bonding resulting in a high barrier for proton displacement. This high barrier also prevents any measurable splitting in the lattice mode frequencies associated with proton tunneling across the potential well, as observed in less tightly-bound hydrogen-bonded crystals.[79]

The statistical distribution of protons in the two equivalent asymmetric positions should likewise not lead to any measurable residual entropy, assuming the presence of only HF molecules and no F^- and $(HFH)^+$ species in the chain. Although the measurement of residual entropy in HF is complicated by the need to evaluate the polymerization entropy in the gas phase, it was concluded on the basis of both spectroscopic and calorimetric measurements[65] that no residual entropy is observed within experimental error.

In further discussions we shall consider the optimized structure, subject to the condition that the R_{FF} distance assumes the experimental value. The most stable structure thus obtained is with $a=1.475$ Å, $d=1.015$ Å, $\alpha=124°$, and $\Delta E=18.1$ kcal/mole.

The experimental sublimation energy at 0°K is difficult to estimate owing to the lack of reliable data to estimate the multimer heat capacity and the equilibrium constants for multimer formation in the gas phase. The thermochemical data measured by Hu *et al.*,[65] together with the data of Simons and Hildebrand[80] for the hexamer formation and that of Briegleb[81] for polymerization rate constants, could be used to give a very rough lower bound of 10.7 kcal/mole for the static cohesive energy. The zero-point energy corrections were estimated by using a simple Einstein Model for each of the optical modes and a Debye model for the acoustical modes. The optical phonon frequencies used are those measured by Kittelberger and Hornig[82] for the zero-phonon wave vector, and the acoustic Debye frequency was taken from the lattice dynamics calculations of Axmann *et al.*[82] Previous calculations on stabilization energies were performed on cyclic hexamers of HF with optimization of intermolecular geometry alone[16] or with the fixed theoretical dimer geometry.[17a] These resulted in a stabilization energy of 12.7 kcal/mole and $R_{FF}=2.22$ Å for a planar structure, with R_{HF} fixed at 0.9384 Å in the minimal basis set calculation,[16] and 10.92 kcal/mole in the INDO calculation with the fixed dimer geometry ($R_{FF}=2.45$ Å and $R_{HF}=1.00$ Å).[17a] No complete structure optimization was previously attempted.

The increase in the intramolecular bond and the bending of the chain observed in this study are characteristic of the hydrogen bond formed. A comparative study made on $(H_2)_n$ chains with identical mesh for the K grid, interaction order, and self-consistency convergence criteria, indicates that upon full minimization of a, d, α, and the out-of-plane angles, the equilibrium structure obtained is the planar chain with $a=1.76$ Å, $d=0.747$ Å (compared with $d=0.746$ Å obtained by the same method for the isolared H_2 molecule), and $\alpha=179°$. The increase in the intramolecular bond and the chain bending are therefore negligible in this structure. On the other hand, structures that involve hybridization between $2s$ and $2p$ orbitals, as $(CH-CH)_n$ chains, are bent.[83]

The band structure of the optimized HF structure with $a=1.475$ Å, $d=1.015$ Å, and $\alpha=180°$ is compared in Fig. 14 with that of the unoptimized crystal structure. The valence bands are shifted to higher energies and the conduction band is shifted to lower energies upon optimization, resulting in a decrease of 3.2 eV in the energy gap and 1.1 eV in the ionization potential. Despite this destabilization of the energy of the occupied one-electron bands, the optimized structure has a larger cohesive energy relative to the unoptimized structure. This results mainly from the effects introduced by the $H_{\mu n,\lambda m}$ matrix elements [Eq. (7)], while

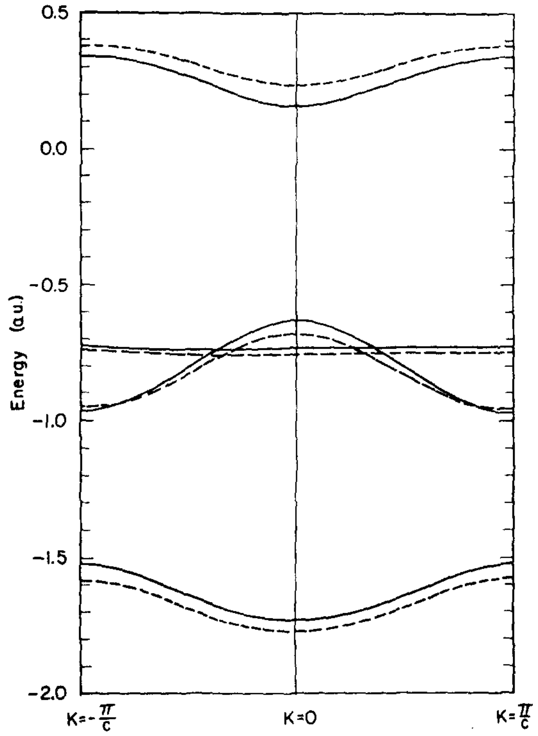

FIG. 14. Band structure of a linear HF crystal: —, optimized structure; $a=1.475$ Å, $d=1.015$ Å; ---, unoptimized structure; $a=1.57$ Å, $d=0.92$ Å.

electron repulsion effects [second term in Eq. (6)] tend to destabilize the optimized structure. The 4σ conduction band is lowered in the optimized structure due to a decrease in its antibonding character. The main effects of stabilization and destabilization occur at the zone center, while at the edges of the BZ, modifications in the bands are less pronounced. The optimized structure is more polar than the unoptimized one owing to a larger charge-transfer accompanying its stabilization.

The intramolecular stretching force constants in the HF crystal were computed by Kittelberger and Hornig[62] in an F – G scheme using the observed ir active stretching vibrational frequencies (antisymmetric mode—3400 cm^{-1}, symmetric mode—3061 cm^{-1}, isolated molecule value—4138 cm^{-1}). The symmetry-adapted force constants thus calculated were 6.5×10^5 dyn/cm and 5.3×10^5 dyn/cm for the antisymmetric and symmetric vibration stretchings, respectively, compared with 9.6×10^5 dyn/cm for the isolated molecule. We calculated stretching force constants by obtaining numerical derivatives of the potential energy corresponding to antisymmetric and symmetric collective proton displacements, in the vicinity of the calculated equilibrium. This yielded 7.2×10^5 dyn/cm and 6.1×10^5 dyn/cm for the antisymmetric and symmetric stretching force constants, respectively, compared with 10.5×10^5 dyn/cm for the isolated molecule. Thus, the clear decrease in stretching force constants upon hydrogen-bond formation is reproduced.

The dependence of the R_{HF} distance on the R_{FF} distance at static equilibrium in the linear chain with $\alpha=180°$ is plotted in Fig. 15. The region where R_{HF} is a decreasing function of R_{FF} is characterized by an asymmetric double minimum in the proton potential, while the region where $R_{HF}=R_{FF}/2$ is characterized by a symmetric single well potential. The transition between these two regions is difficult to establish accurately, owing to the shallowness of the potential, and is indicated in Fig. 15 by the shaded area. A similar experimental correlation was observed by Pimentel and McClellan in O–H···O bonds[31] and calculated by the phenomenological O–O, O–H, and O···H potentials by Reid.[20] It is interesting to speculate on the nature of the proton positions in fluorine hydrogen-bonded solids in view of this calculation. This leads to $LiHF_2$ ($R_{FF}=2.27$ Å),[84] KHF_2 ($R_{FF}=2.26$ Å),[85] and NH_4HF_2 ($R_{FF}=2.272$ Å)[86] being characterized by a symmetric hydrogen bond, while KH_2F_3 ($R_{FF}=2.33$ Å)[87] is a border case having either a single symmetric minimum or a very low barrier in a double-minimum well. Neutron diffraction data are presently available only for KHF_2,[88] indicating indeed a central position for the hydrogen atoms. Similar correlations between F–F distance and the lattice skeletal vibration frequency were suggested by Boutin *et al.*[64a]

The fluorine net charges as a function of proton location in the chain are shown in Fig. 16 for various R_{FF} distances. It is observed that the largest charge transfer occurs for central proton positions, in which the proton polarizes its nearest fluorine atoms equally. For all R_{FF} values, the fluorine charge decreases approaching the corresponding free molecule value as the protons are more asymmetric. As the F–F distance decreases, the equilibrium proton positions tend to become closer to the center of the F–F bond, and the fluorine charge becomes strongly more negative.[64a] This should increase the magnitude of the dipole moment for F–H stretching resulting in an enhancement of the intensity of the vibration.

We next examine the stability of the structure that we optimized with respect to unit cell parameters (out-of-

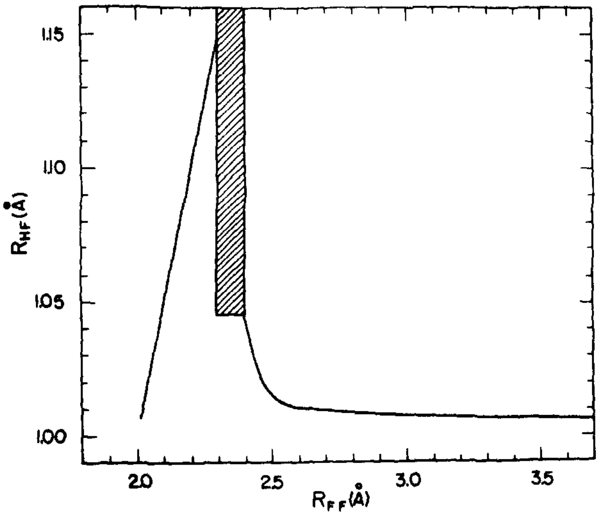

FIG. 15. Dependence of R_{HF} or R_{FF} at static equilibrium, for the linear chain with $\alpha=180°$.

plane angles, chain angle, and R_{HF} keeping R_{FF} constant at the experimental value), against displacement of a *specific* proton. Figure 17 shows the variation in the crystal potential (relative to the equilibrium of the unit cell) due to the displacement $R_H = (\frac{1}{2}R_{FF} - R_{HF})$ of a specific proton from its equilibrium position, while all other protons are kept in their usual asymmetric positions. The proton that was initially at $R_H = 0.23$ Å in the perfect lattice tends to return to this position. The energy required to move this proton to $R_H = 0.23$ Å, thus forming an ionic Bjerrum defect composed of a symmetric $(HFH)^+$ pair and a F^- anion, is 83.90 kcal/mole. This defect is formed by rotation of a specific HF molecule in the crystal by 180° about its center or by the tunneling of a single proton to the opposite side of its potential well. The broken curve in Fig. 17 shows the potential energy of the crystal due to displacement of a specific proton while all other protons are kept in the *symmetric* positions, midway between two neighboring fluorine atoms.

Several conclusions may be drawn from these results:

(1) When all protons are in their asymmetric equilibrium positions, the crystal is stable against displacement of a single proton.

(2) The displacement of a specific proton between its neighboring fluorine atoms in the F_1–H$\cdots F_2$ structure is critically dependent on the positions of all other protons in the crystal. This conclusion is validated by calculating the potential for a specific proton displacement, when the protons up to the Jth neighbors of the specific proton are in the equilibrium asymmetric position and all other protons (from the Jth to the 10th neighbors) are in a symmetric position. The unbroken curve in Fig. 17 corresponds to $J = 10$ and the broken one to $J = 0$. It is observed that starting for J greater than 2, the system exhibits an increasing asymmetry, resulting finally in the stable and strongly asymmetric structure for $J = 10$. This implies that a relatively long-range proton–proton coupling exists in this hydrogen-bonded system.[54] This results in a dependence of the forces acting on one proton, on the positions of other, rather distant, protons. This coupling is very similar to that suggested by Löwdin in the collective motion of protons in enzymes[89] and to the long-range coherence discussed by Frölich.[90]

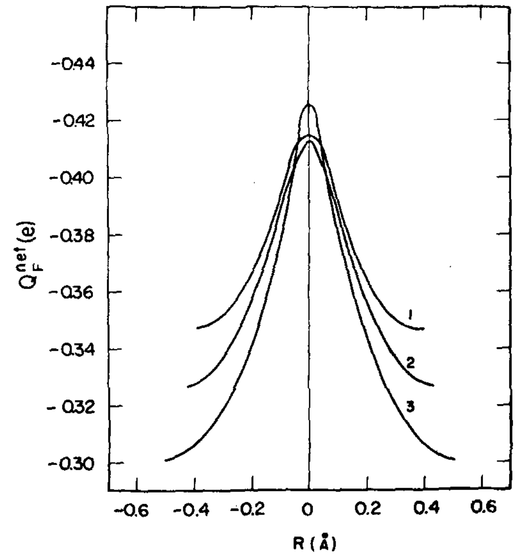

FIG. 16. Fluorine net atomic charge as a function of proton position $R = (\frac{1}{2}R_{FF} - R_{HF})$ in the chain, for several R_{FF} distances: R_{FF} = (1) 2.00 Å, (2) 2.25 Å, (3) 2.73 Å.

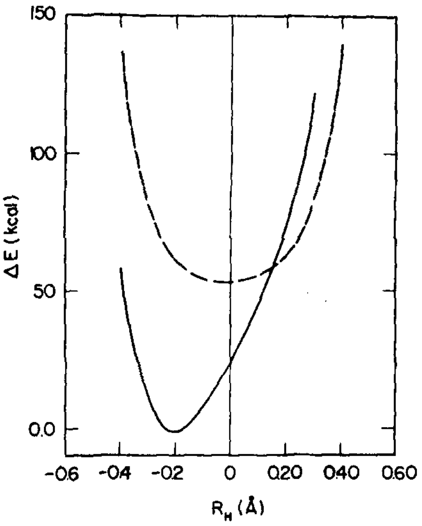

FIG. 17. Potential energy for specific proton displacement in an HF chain: –, all protons in asymmetric positions; $a = 1.475$ Å, $d = 1.015$ Å; ---, all protons in symmetric positions; $a = d = 1.245$ Å.

(3) The central position of all protons is characterized by a very small force constant for proton displacement (upper curve, Fig. 17). Alternatively, as more neighboring molecules are situated in symmetric positions around an asymmetric proton, the force constant determining its motion decreases. Collective proton displacements can thus occur in such a chain structure by successive polarization of each proton by its neighboring protons. This motion is probably very inefficient in HF crystals at low temperatures owing to the large energy involved in proton displacements in this strongly hydrogen-bonded system, but could probably take place in systems with weaker bonds.

(4) Theories that do not account for long-range proton coupling, like the methods employing phenomenological atom–atom potentials with either no proton–proton coupling[19,20] or with a strongly decaying (Lennard–Jones or Buckingham) potential,[24] are probably unsuitable for describing extended hydrogen–bonded structures exhibiting collective properties.

V. SUMMARY AND CONCLUSIONS

The small-periodic-cluster method suggested permits both the calculation of the electronic structure of a perfect lattice and that of systems lacking full translational symmetry due to displacements of one or more atoms from substitutional sites. The method is thus capable of treating band structure as well as conformational aspects and point defect structure. The main conclusions that can be drawn from this work are as follows:

(1) Conventional tight-binding calculations employing unperturbed free-molecule charge densities or electrostatic potentials and neglecting crystal-field effects are inadequate for hydrogen-bonded solids such as HF, in view of the large charge residtribution accompanying the intra- and intermolecular rearrangements during the bond formation.

(2) In computing the interaction matric elements, one should employ at least 5–6 K-grid points in the BZ sums and more than 3–5 orders of neighbors in the lattice sums to obtain stable bands. Likewise, the importance of both intra- and intermolecular self-consistency in the calculations is demonstrated.

(3) Truncated-crystal models are inadequate for treating the electronic structure of such hydrogen-bonded crystals, unless a very large number of molecules is employed. Edge effects, characterized by a strong charge inhomogeneity at the surface, propagate quite deep into the bulk of the cluster, thereby perturbing the perfect lattice properties to a significant extent. Thus, application of periodic boundary conditions cannot be avoided. Systems that exhibit smaller charge rearrangement upon formation from isolated molecules (molecular van der Waals solids) are probably more amenable to truncated-crystal models.

(4) The potential energy and electrostatic interactions of a proton between two neighboring electronegative atoms are critically dependent on the configuration of other protons. Phenomenological models employing atom–atom interactions with either no H–H potential or with a strongly decaying covalent H–H potential are likely to be unsuitable for such hydrogen-bonded system.

(5) The use of the semiempirical all-valence electron INDO method in conjunction with the small-periodic-cluster representation is easy to implement in practice and yields, with reasonable computing time, a wealth of information regarding electronic energies, charges, etc. However, owing to the inherent approximations underlying the INDO method, only semiquantitative information can be obtained on properties such as equilibrium conformation. If more accurate results are required, *ab initio* methods cannot be avoided.

The general aspects of the hydrogen bonds in solid HF (formation of disperse energy bands, intramolecular bond relaxation, decrease in stretching force constants, asymmetry of the proton potential, etc.) are clearly demonstrated. Further experiments on optical properties, photoelectron scattering, neutron diffraction, and dielectric relaxation would serve to further clarify these electronic and structural features of the hydrogen bond in solid HF.

---

[1] F. Bassani, L. Pietronero, and R. Resta, J. Phys. C 6, 2133 (1973).

[2] G. P. Parravicini and L. Resta, Phys. Rev. B 8, 3009 (1973).

[3] J. Lennard-Jones and J. A. Pople, Proc. R. Soc. Lond. A 205, 155 (1951).

[4] M. M. Jones. W. R. Gilkerson, and G. A. Gallup, J. Chem. Phys. 20, 1048 (1952).

[5] W. G. Schneider, J. Chem. Phys. 23, 26 (1955).

[6] R. F. W. Bader, Can. J. Phys. 42, 1822 (1964).

[7] B. Z. Howard, J. Chem. Phys. 39, 2524 (1963).

[8] C. A. Coulson and U. Danielsson, Ark. Fys. 8, 245 (1954).

[9] H. Tsubomura, Bull, Chem. Soc. Jpn. 27, 445 (1954).

[10] S. Bratoz, *Advances in Quantum Chemistry*, edited by P. O. Löwdin (Academic, New York, 1967), Vol. 3, p. 209.

[11] P. G. Puranic and V. Kumar, Proc. Indian Acad. Sci. 58, 29 (1963).

[12] E. Clementi and A. D. McLean, J. Chem. Phys. 36, 745 (1962).

[13] G. H. F. Diercksen and W. P. Kraemer, Chem. Phys. Lett. 6, 419 (1970).

[14] J. Almlof, Chem. Phys. Lett. 17, 49 (1972).

[15] M. Dreyfus and A. Pullman, Theor. Chim. Acta 19, 20 (1970).

[16] J. E. Del-Bene and J. A. Pople, J. Chem. Phys. 55, 2296 (1971).

[17] (a) P. A. Kollman and L. C. Allen, J. Am. Chem. Soc. 92, 753 (1970); (b) P. A. Kollman and L. C. Allen, J. Chem. Phys. 52, 5085 (1970).

[18] J. R. Sabin, J. Chem. Phys., 56, 45 (1972).

[19] E. R. Lippincott and R. Schroeder, J. Chem. Phys., 23, 1099 (1955)

[20] C. Reid, J. Chem. Phys., 30, 182 (1959).

[21] R. A. Scott and H. A. Scheraga, J. Chem. Phys., 45, 2091 (1966).

[22] C. Dosi, E. Giglio, V. Pavel and C. Quaglita, Acta Crystallogr., Sect A 29, 644 (1973).

[23] D. A. Brant, Macromolecules 1, 291 (1968).

[24] A. T. Hagler, E. Huler and S. Lifson, J. Amer. Chem. Soc., in press.

[25] B. Grahn, Ark. Fys. 15, 257 (1959).

[26] P. O. Löwdin, Advan. Phys., 5, 1 (1956)

[27] M. Roux, S. Bernainou and R. Daudel, J. Chim. Phys., P. 218 (1956).

[28] F. P. Larkins, J. Phys. C., 4, 3065, 3077 (1971).

[29] R. P. Messmer and G. D. Watkins, Phys. Rev. B., 7, 2568 (1973).

[30] A. Zunger, (a) J. Phys. C. (London) 7, 76 (1974), (b) Mol. Phys., in press, (1974).

[31] G. C. Pimentel and A. L. McClellan, *The Hydrogen Bond* (W. H. Freeman, San Francisco, 1960), p. 260.

[32] S. N. Vinogradov and R. H. Linnell, *Hydrogen Bonding* (Van Nostrand–Reinhold, New York, 1971), p. 176.

[33] W. C. Hamilton and J. A. Ibers, *Hydrogen Bonding In Solids* (Benjamin, New York, 1968), p. 52.

[34] L. Pietronero, Note No. 437, Instituto di Fisica G. Marconi, Universita di Roma (1973).

[35] A. Zunger, J. Phys. C 7, 96 (1974).

[36] A. Zunger, J. Chem. Phys. (in press).

[37] A. Zunger (in preparation).

[38] R. S. Mulliken, J. Chem. Phys. 56, 792 (1952).

[39] (a) D. M. Dorst and J. L. Fry, Phys. Rev. B 5, 684 (1972); (b) D. L. Beveridge, I. Jano, and J. Ladik, J. Chem. Phys. 56, 4744 (1972); (c) J. M. Andre, J. Chem. Phys. 50, 1536 (1969); (d) T. L. Gilbert, *Molecular Orbits in Chemistry, Physics and Biology*, edited by O. Sinanoglo (Yale U. P., New Haven, CT, 1964), p. 405; (e) J. Callaway and J. L. Fry, *Computational Methods of Band Theory*, edited by P. M. Marcus, J. F. Janak, and A. R. Williams (Plenum, New York, 1971), p. 512.

[40] (a) W. D. Connolly, Phys. Rev. 159, 931 (1967); (b) W. E. Rudge, Phys. Rev. 181, 1024 (1969).

[41] D. J. Stukel and R. Euwema, Phys. Rev. B 1, 1635 (1970).

[42] (a) G. K. Koster and J. C. Slater, Phys. Rev. 95, 1167 (1954), and 96, 1208 (1954); (b) F. Bassani, G. Iadonisi, and B. Preziosi, Phys. Rev. 186, 735 (1969); (c) K. H. Bennemann, Phys. Rev. A 137, 1497 (1965).

[43] (a) C. A. Coulson and M. J. Kearsley, Proc. R. Soc. A 241, 433 (1957); (b) B. S. Gourary and A. E. Fein, J. Appl. Phys. 33, 331 (1962).

[44] For example, see A. S. N. Murthy and C. N. R. Rao, Chem. Phys. Lett. 2, 123 (1968); also W. Adams, A. Grimson, R. Hoffman, and C. Ortiz, J. Am. Chem. Soc. 90, 1509 (1968).

[45] (a) G. Blyholder and C. A. Coulson, Theor. Chim. Acta 10, 316 (1968); (b) L. C. Allen and J. D. Russel, J. Chem. Phys. 46, 1029 (1967).

[46] J. A. Pople and D. L. Beveridge, in *Approximate M. O. Theory* (McGraw-Hill, New York, 1970).

[47] R. K. Nesbet, J. Chem. Phys. 36, 1518 (1962).

[48] R. Weiss, Phys. Rev. 131, 659 (1963).

[49] B. J. Ransile, Rev. Mod. Phys. 32, 245 (1960).

[50] A. D. McLean and M. Yoshimine, J. Chem. Phys. 47, 325 (1967).

[51] J. E. Bloor and Z. B. Muksic, Mol. Phys. 22, 351 (1971).

[52] D. E. Stogryn and A. P. Stogryn, Mol. Phys. 11, 371 (1966).

[53] R. P. Hurst, M. Karplus, and T. P. Das, J. Chem. Phys. 36, 2786 (1962).

[54] R. N. Spanbauer, K. N. Rao, and L. H. Jones, J. Mol. Spectrosc. 16, 100 (1965); and D. V. Webb and K. N. Rao, J. Mol. Spectrosc. 28, 121 (1968).

[55] P. J. Wilkinson, Astrophys. J. 138, 778 (1963).

[56] H. L. Lempka and W. C. Price, J. Chem. Phys. 48, 1875 (1968).

[57] G. Herzberg, *Molecular Spectra and Molecular Structure I. Spectra of Diatomic Molecules* (Van Nostrand, Princeton, NJ, 1950).

[58] G. H. Diercksen and W. P. Kaemer, Chem. Phys. Lett. 6, 419 (1970).

[59] T. R. Dyke, B. J. Howard, and W. Klemperer, J. Chem. Phys. 56, 2442 (1972).

[60] D. F. Smith, J. Mol. Spectrosc. 3, 473 (1959).

[61] M. Atoji and W. N. Lipscom, Acta Crystollogr. 7, 173 (1954).

[62] J. S. Kittelberger and D. F. Hornig, J. Chem. Phys. 46, 3099 (1967).

[63] M. L. N. Sastri and D. F. Hornig, J. Chem. Phys. 39, 3497 (1963).

[64] (a) H. Boutin, G. J. Safford, and V. Brajovic, J. Chem. Phys. 39, 3135 (1963); (b) H. Boutin and G. J. Safford, in *Inelastic Scattering of Neutrons* (IAEC, Vienna, 1965), Vol. 2, p. 393.

[65] J. H. Hu, D. White, and H. L. Johanston, J. Am. Chem. Soc. 75, 1232 (1953).

[66] S. P. Habuda and Y. V. Gagarinsky, Acta Crystallogr. B 27, 1677 (1971).

[67] C. W. Kern and M. Karplus, J. Chem. Phys. 40, 1374 (1964).

[68] S. Srebrenik, H. Weistein, and R. Paunz, Chem. Phys. Lett. 20, 419 (1973).

[69] W. J. Hehre, R. F. Stewart, and J. A. Pople, J. Chem. Phys. 51, 2657 (1969).

[70] C. Giessner-Prettre and A. Pullman, Theor. Chim. Acta 25, 83 (1972).

[71] (a) R. Bonaccorsi, A. Pullman, E. Scrocco, and J. Tomasi, Theor. Chim. Acta 24, 51 (1972); (b) E. Scrocco and J. Tomasi, J. Chem. Phys. 52, 5270 (1970).

[72] K. Morokuma and L. Petersen, J. Chem. Phys. 48, 3275 (1968).

[73] P. A. Kollman and L. C. Allen, J. Chem. Phys. 51, 3286 (1969).

[74] L. Piela, L. Pietronero, and R. Resta, Phys. Rev. B 7, 5321 (1973).

[75] J. D. Levine, Phys. Rev. 174, 911 (1968).

[76] S. G. Davison and J. Koutecky, Proc. Phys. Soc. 89, 237 (1966).

[77] (a) W. H. Harrison, *Pseudopotentials in the Theory of Metals* (Benjamin, New York, 1966); (b) F. Bassani and G. P. Parravicini, Nuovo Cimento 50, 95 (1967).

[78] J. C. Slater and F. G. Koster, Phys. Rev. 94, 1495 (1954).

[79] See, for instance, R. L. Somorjai and D. F. Hornig, J. Chem. Phys. 36, 1980 (1962); and R. G. Snyder and J. A. Ibers, J. Chem. Phys. 36, 1356 (1962).

[80] J. Simons and J. H. Hildebrand, J. Am. Chem. Soc. 46, 2183 (1974).

[81] G. Briegleb, Z. Phys. Chem. B 51, 9 (1941).

[82] A. Axmann, B. Biem, P. Borsch, F. Hobfeld, and H. Stiller, Discuss. Faraday Soc. 48, 69 (1969).

[83] S. O'Shea and D. P. Santry, J. Chem. Phys. 54, 2667 (1971).

[84] L. K. Freud and H. W. Rinn, Acta Crystallogr. 15, 786 (1962).

[85] L. Helmholz and M. T. Rogers, J. Am. Chem. Soc. 61, 2590 (1939).

[86] T. R. R. McDonald, Acta Crystallogr. 13, 113 (1960).

[87] J. D. Forrester, M. E. Senko, A. Zalkin, and D. H. Templeton, Acta Crystallogr. 16, 58 (1963).

[88] S. W. Peterson and H. A. Levy, J. Chem. Phys. 20, 704 (1952).

[89] P. O. Löwdin, Biopolym. Symp. 1, 293 (1964).

[90] M. Frölich, Int. J. Quant. Chem. 2, 641 (1968).